Pre-salt rift morphology controls salt tectonics in the Campos Basin, offshore SE Brazil

Francyne Bochi do Amarante[1,2,#]

[1] Instituto de Geociências, Universidade Federal do Rio Grande do Sul, Porto Alegre, 90650 001, Brazil

[2] Basins Research Group (BRG), Department of Earth Science and Engineering, Imperial College London, London, SW7 2BP, United Kingdom

[#] corresponding author francyne.amarante@ufrgs.br

ORCID https://orcid.org/0000-0003-4452-8635

Christopher Aiden-Lee Jackson[2]

[2] Basins Research Group (BRG), Department of Earth Science and Engineering, Imperial College London, London, SW7 2BP, United Kingdom

c.jackson@imperial.ac.uk

ORCID https://orcid.org/0000-0002-8592-9032

Leonardo Muniz Pichel[2,3]

[3] Department of Earth Science, University of Bergen, Allegaten 41, 5007, Bergen, Norway

leonardo.m.pichel@uib.no

ORCID https://orcid.org/0000-0001-8692-3831

Claiton Marlon dos Santos Scherer[1]

[1] Instituto de Geociências, Universidade Federal do Rio Grande do Sul, Porto Alegre, 90650 001, Brazil

claiton.scherer@ufrgs.br

ORCID https://orcid.org/0000-0002-7520-1187

Juliano Kuchle[1]

[1] Instituto de Geociências, Universidade Federal do Rio Grande do Sul, Porto Alegre, 90650 001, Brazil

juliano.kuchle@ufrgs.br

ORCID https://orcid.org/0000-0003-4325-0547

Abstract

Classic models of gravity-driven salt tectonics commonly depict kinematically-linked zones of overburden deformation, characterised by updip extension and downdip contraction, separated by a weakly deformed zone associated with downdip translation above a relatively smooth base-salt surface. We use 2D and 3D seismic reflection and borehole data from the south-central Campos Basin to show that these models fail to adequately capture the complex range of structural styles forming during salt-detached gravity-driven deformation above a rugose base-salt surface. In the Campos Basin the base-salt is defined by broadly NE-trending, margin-parallel, generally seaward-dipping ramps that have up to 2 km of structural relief. We define three domains of overburden deformation: an updip extensional domain, an intermediate multiphase domain, and a downdip contractional domain. The multiphase domain is defined by large, partly fault-bounded, ramp-syncline basins, the stratigraphic record of which suggest c. 28 km of seaward gravity-driven translation of salt and its overburden since the end of the Albian. We also identify three main types of salt structures in the multiphase domain: (i) contractional anticlines that were subjected to later extension and normal faulting; (ii) passive-to-active diapirs that were later extended and widened, and which are bound on their landward margins by landward-dipping, salt-detached normal faults; and (iii) reactive (extensional) diapirs that were subsequently squeezed. We argue that this multiphase deformation occurs because of basinward translation of salt and its overburden over complex base-salt relief, consistent with the predictions of physical models and several other seismic reflection data-based studies. Critically, these complex local strains overprint margin-scale patterns of deformation.

Keywords: base-salt relief, rift basin, passive margin, South Atlantic basins, ramp syncline basins, gravity-driven deformation, salt translation.

1 - Introduction

Salt-bearing passive margins typically deform in response to gravity gliding and gravity spreading (Peel, 2014). Such margins can be divided into kinematically linked domains of deformation, each associated with a distinct suite of salt and overburden structures (e.g. Rowan et al., 2004; Brun and Fort, 2011; Peel, 2014). The upslope domain is characterised by thin-skinned (i.e. salt-detached) extension, which is associated with the formation of listric normal faults, rafts, and salt rollers (e.g. Lundin, 1992; Brun and Mauduit, 2009; Jackson and Hudec, 2017). Updip extension is accommodated by and kinematically linked to downdip contraction and the formation of salt-cored anticlines and salt-detached thrusts (e.g. Demercian et al., 1993; Brun and Fort, 2004; Fort et al., 2004). Domains of extension and contraction are separated by a domain of translation, in which deformation is typically described as being relatively mild (Brun and Fort, 2004; Davison et al., 2012).

Recent studies on South Atlantic salt basins have demonstrated that this structural zonation is an oversimplification. More specifically, these studies show that various extensional and contractional structures, in addition to ramp-syncline basins (RSBs), can form in the translational domain due to the flow of salt and overburden across base-salt relief associated with prior rifting (Brun and Fort 2004, 2011; Dooley et al., 2017; Hudec et al., 2013; Pichel et al., 2018, 2019a; Evans and Jackson, 2020; Erdi and Jackson, 2021). Local deformation can overprint regional patterns of deformation, resulting in multiphase structures with a complex kinematic history (Dooley et al., 2017; Pichel et al., 2019b; Erdi and Jackson, 2021).

The Aptian salt basin offshore southeastern Brazil contains substantial volumes of hydrocarbons and, because of this, has been intensively studied by the energy industry since the 1970's (e.g. Guardado et al., 1989; Mohriak et al., 1990; Bruhn et al., 2003). There are presently 62 producing hydrocarbon fields in the Campos Basin (ANP, 2020). These fields relate to at least four petroleum systems, with reservoirs in pre- and intra-salt (i.e., pre-Aptian

and Aptian) clastics and carbonates, post-salt (Albian-Cenomanian) marine carbonates, and most importantly, Upper Cretaceous to Miocene clastic turbidites (Guardado et al., 1989; Bruhn et al., 2003). The deposition and deformation of salt have strongly controlled the development of petroleum systems in the Campos Basin (Guardado et al., 1989; Mohriak et al., 2012). For example, salt can be the seal rock, mainly to rift and Aptian pre-salt accumulations, and salt structures (more specifically thin-skinned faulting above salt anticlines and rollers) can form traps to post-salt sediments. The absence of salt, for example along welds, can define pathways for hydrocarbon migration, and salt-related faults can act as both migration pathways or traps, depending on their location and stratigraphic level. Despite its importance, there are surprisingly few international publications on the salt tectonics of the Campos Basin (Cobbold and Szatmari, 1991; Demercian et al., 1993; Rouby et al., 1993; Mohriak et al., 2008 Davison et al., 2012; Quirk et al., 2012), and only a few present a detailed, regional-scale analysis of the geometry and kinematics of the salt and overburden structures (Demercian et al., 1993; Rouby et al., 1993). An improved knowledge of salt tectonics is required to understand the timing and style of salt-related deformation and deposition, and to extend hydrocarbon exploration further basinward into deeper waters.

In this study we use 2D and 3D seismic reflection and borehole data to characterise the salt-tectonic structural styles and related evolution of salt and overburden structures in the south-central Campos Basin, SE Brazil. We first describe the extensional and contractional domains, before focusing on the boundary between the two, which we herein name the *multiphase domain*. We then investigate the evolution of extensional and contractional deformation through time and space. We conclude by discussing the effects of base-salt relief on the distribution, origin and evolution of salt and overburden structures, and the implications of our work for post-salt hydrocarbon exploration in the deep-water Campos Basin.
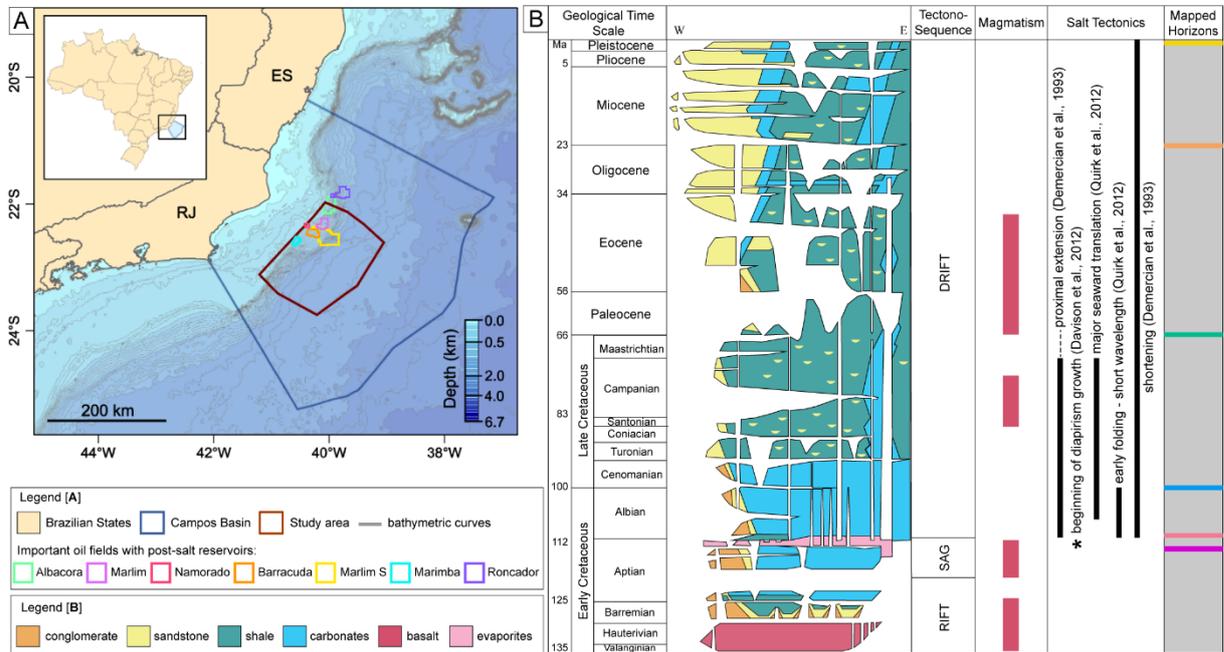
2 - Geological Context

The Campos Basin (c. 100,000 km²) is located on the southeastern Brazilian margin, offshore the states of Rio de Janeiro and Espírito Santo (Figure 1a) (Guardado et al., 1989; Winter et al., 2007). The basin originated during rifting of the Gondwana Supercontinent that culminated in the opening of the South Atlantic Ocean in the Late Jurassic-to-Early Cretaceous (Figure 1b) (Szatmari, 2000). The basin is limited to the north by the Vitória High, to the south by the Cabo Frio High (Figure 2a), to the east by oceanic crust, and to the west by exposures of crystalline basement rocks of the Ribeira Belt (Mohriak et al., 1989; Heilbron et al., 2000).

The syn-rift stage of the Campos Basin (Valanginian – Early Aptian) (Figure 1b) initiated at ~135 Ma with intense volcanic activity, coeval with the Serra Geral volcanism documented in the Paraná Basin (Baksi, 2018). Rifting was associated with the formation of NE-SW-striking normal faults that bound structural highs (horsts) and structural lows (grabens), including the External High and the External Low (Figure 2a) (Chang et al., 1992; Guardado et al., 2000). The inner (i.e. marginal) hinge line of the rift system is delineated by the Campos Fault (Figure 2a), a large structure that separates the shallow, western part, where Tertiary deposits rest directly on basement, from the deeper, eastern portion, where relatively thick accumulations of Barremian to Aptian sediment fill rift-related depocentres (Figure 2c) (Guardado et al., 1989).

The early post-rift (i.e. sag) stage commenced in the Aptian (Figure 1b), marking the transition from basement-involved faulting and relatively rapid subsidence, to a period defined by very little faulting and long-wavelength, relatively slow subsidence driven by post-rift cooling of the lithosphere. Because of this change in subsidence pattern and rate, the depositional area enlarged and sedimentation progressively draped and essentially 'healed' rift-related relief (Quirk et al., 2013; Kukla et al., 2018; Amarante et al., 2020). During the late Aptian, a thick salt layer was deposited in response to episodic marine-water influx through the

Walvis Ridge volcanic high to the south (Davison et al., 2012). Even though salt deposition occurred late in the sag phase, relief inherited from the rift phase still locally influenced salt distribution (Davison et al., 2012; Dooley et al., 2017).

Figure 1. (A) Regional map showing the location of Campos Basin, the study area polygon and the main oil fields with post-salt reservoirs. (B) Simplified stratigraphic chart of Campos Basin (redrawn from Winter et al., 2007), with the main magmatic events and timing of the salt tectonics from previous publications; the last column shows the mapped horizons of this study with their designed colours.

The end of evaporite deposition is marked by a rapid marine transgression linked to the initiation of the drift (i.e. late post-rift) stage (Albian – Present) (Figure 1b) (Chang et al., 1992). Focusing of thermally induced subsidence near the location of continental breakup caused the basin to tilt southeastward, inducing gravity gliding of Aptian salt and its overburden (Quirk et al., 2012). Major progradation of basin-margin clastic wedges, linked to continental uplift and erosion, commenced in the Eocene and continues to the present day (Contreras et al., 2010).

Salt-related deformation in the central South Atlantic region began in the Aptian (i.e. *during* salt deposition; Figure 1b) (Cobbold and Szatmari, 1991; Fiduk and Rowan, 2012; Davison et al., 2012), with the major seaward flow of salt and its overburden continuing until the Maastrichtian (Figure 1b) (Quirk et al., 2012). Based on salt (and overburden) structural style, the Campos Basin is divided into a proximal extensional domain (70 - 200 km wide) and

a distal contractional domain (70 - 300 km wide), the latter terminating seaward in a broad (up to 37 km wide) allochthonous salt sheet emplaced on the outer basement high (Figures 2b and 2c) (Davison, 2007; Davison et al., 2012). Previous works identify rafts, salt rollers, extensional anticlines, triangular-shaped (reactive) salt walls, and collapsed diapirs in the extensional domain, with all of these structures related, in some way, to landward- and seaward-dipping, salt-detached normal faults (Demercian et al., 1993; Mohriak et al., 2008; Quirk et al., 2012). Further seaward in the translation domain, Dooley et al. (2017) describe a large RSB. The contractional domain is characterized by elongate salt walls (Demercian et al., 1993) and polyharmonic, salt-detached (buckle) fold belts (Cobbold and Szatmari, 1991; Dooley et al., 2017).
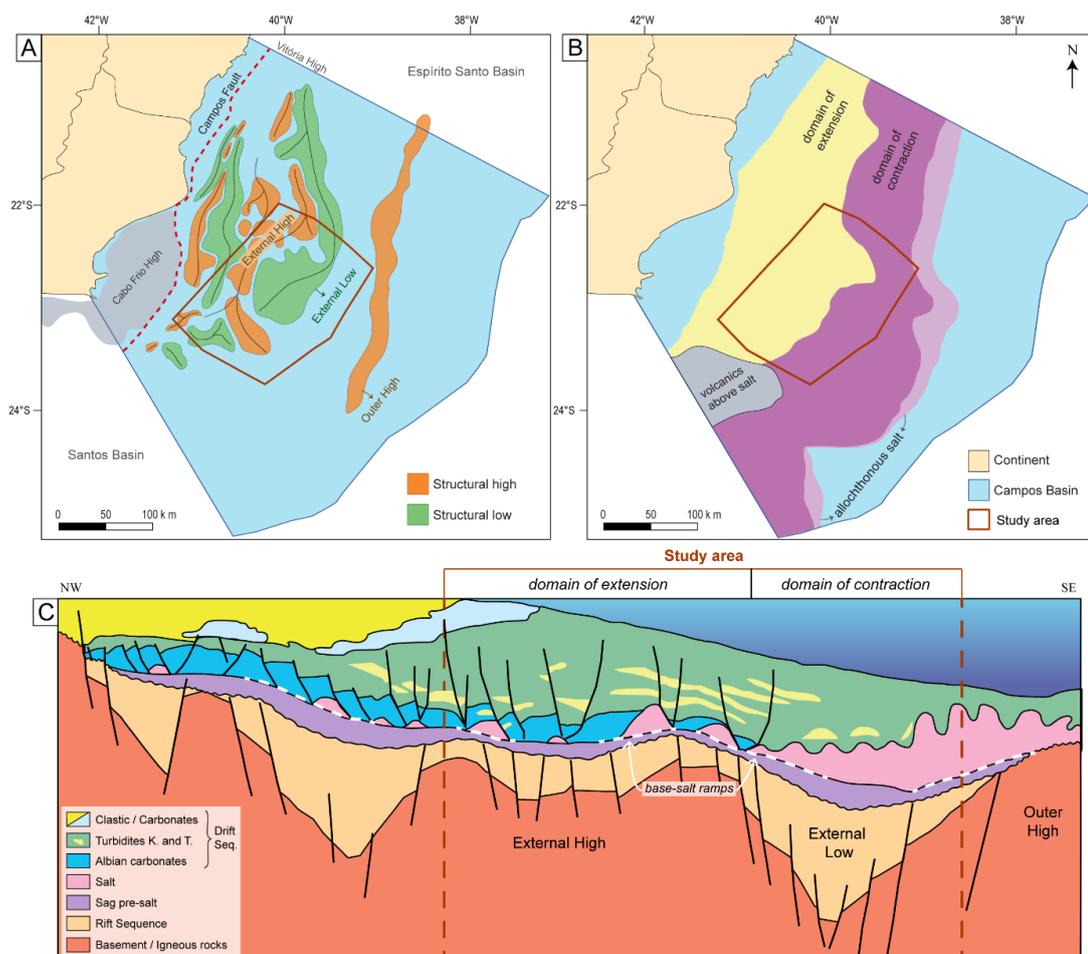

Figure 2. (A) Pre-salt structural framework of Campos Basin, redrawn from Guardado et al. (2000); Outer High and Cabo Frio High locations from Fetter (2009). (B) Salt-related structural provinces, modified from Davison et al. (2012); volcanics above salt location from Meisling et al. (2001). (C) Schematic cross section of Campos Basin, modified from Rangel et al., 1994.

3 - Database and Methodology

Our seismic reflection database comprises 146 2D lines and one 3D volume from the ANP (Brazil's National Oil, Natural Gas and Biofuels Agency) data library, covering an area of c. 23,500 km² of the central-southern platform of Campos Basin (Figures 1a and 3). Spacing between the 2D seismic lines ranges from around 1 to 30 km. The 3D volume covers c. 2,900 km², with inlines (east-west) and crosslines (north-south) spaced 12.5 m (Figure 3). The seismic surveys are time-migrated (PTSM Kirchoff), zero-phase processed, with a display following SEG "normal" polarity; i.e. a downward increase in acoustic impedance is represented by a positive reflection event (i.e. white on displayed seismic profiles). All seismic lines and mapped horizons (see below) are presented in two-way travel time (TWT) milliseconds (ms) and have not been depth-converted, meaning we describe relative rather than absolute changes in, for example, thicknesses between and within stratigraphic units, and changes in dip along seismically defined surfaces.

Within the study area there are 30 boreholes that contain well-logs (e.g. sonic travel time, bulk density, and gamma ray), and stratigraphic (i.e. age) and lithology data that help us constrain the age of the mapped horizons and the composition of the seismic-stratigraphic units they bound. These wells were tied to the seismic data through checkshot surveys. The interval velocity of the Aptian evaporites obtained from the well-logs ranges from 4000 to 7000 m/s depending on the proportion of halite, anhydrite, and potash salts. Overburden strata are defined by interval velocities ranging from 1800 to 6000 m/s due to the highly varying densities of different lithologies (e.g. mudstone, sandstones, conglomerates, carbonates) with varying porosities. We estimate that the vertical seismic vertical resolution in the interval of interest is 10 to 50 m; this is sufficient to map the kilometer-scale salt-related structures that form the focus of this study.
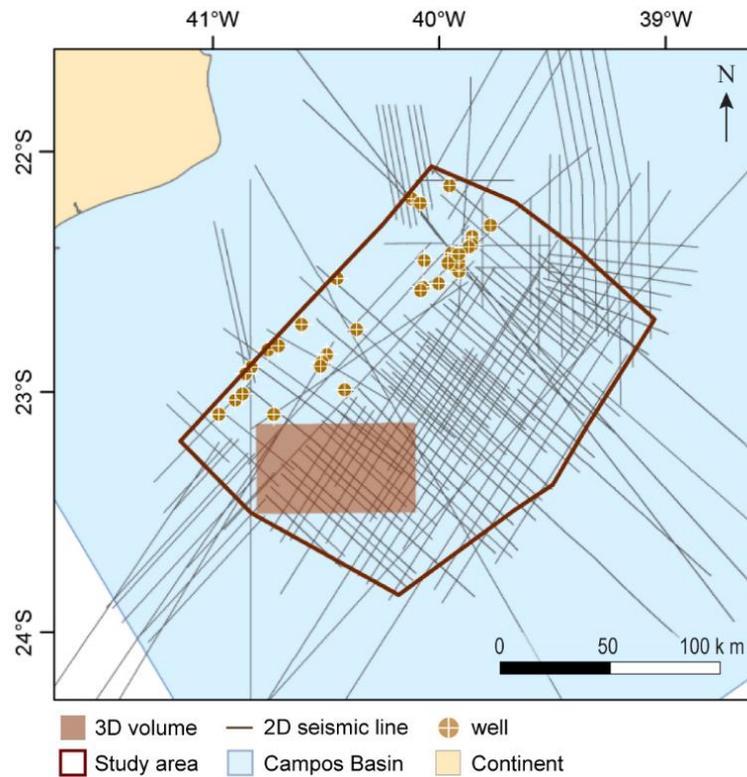
Figure 3. Dataset used in this study: 146 2D lines (or lines segments), one 3D volume and 30 boreholes.

In addition to the seabed, we mapped four key horizons across the dataset: base of salt, top of salt, top Cretaceous, and top Paleogene. Where possible, we mapped the top Albian (Figure 1b). We mapped the top Cretaceous and top Paleogene horizons because they represent regional seismic-stratigraphic unconformities that are easily identifiable throughout the Campos Basin and which record major periods of salt-related deformation. The mapped surfaces display the present basin geometry, whereas isochron (i.e. thickness) maps derived from these surfaces show the distribution and evolution of salt-related sedimentary depocentres, allowing us to infer salt kinematics and dynamics.

Evaporites are generally defined by significantly higher seismic velocities than encasing sedimentary rocks. In time-migrated seismic sections, thick salt structures may be underlain by velocity pull-ups in the base-salt surface and underlying, sub-salt reflections. Velocity pull-ups mimic the geometry of the overlying salt structures and may erroneously be interpreted as sub-salt structural highs (Marfurt and Alves, 2015). Such seismic artifacts occur in the SE portion of the study area where high-relief salt structures are present (Figure 4a); we therefore manually

corrected our interpretation of the base-salt horizon to compensate for these pull-ups (Figure 4b). We then mapped the base-salt ramps and calculated the dip-angle of these ramps in varying locations (Figure 4c), converting time (TWT, ms) to depth using a velocity of 4600 m/s (i.e. the average interval velocity of the underlying rocks calculated from the well logs). Local base-salt dip angles were also calculated using the same methodology (Figure 4d).

We chose the most representative, dip-oriented seismic profile to perform a structural restoration and develop a balanced kinematic model for the salt tectonics in the study-area. We combine decompaction and unfolding by simple vertical shear, and move-on-fault algorithms, following established restoration workflows for salt-related deformation (see Rowan and Ratliff 2012, Pichel and Jackson, 2020). The profile is restored to a gently dipping (~1°), clinoform-like seabed, characteristic of the prograding margin of the Campos Basin (cf. Figures 2c and 8). We reconstruct the approximate palaeo-seabed through time using the present seabed as a template, and local erosional unconformities and toplaps as additional constraints (cf., Pichel and Jackson, 2020). Decompaction is performed using the Sclater and Christie (1980) function, assuming a clastic-dominated (i.e. post-Albian) overburden; this assumption is supported by lithological data provided by the available boreholes, and by previous studies (Winter et al., 2007; Contreras et al., 2010). Note that we did not depth-convert the time-migrated seismic profile and that the restored sections are shown with 2-3 times vertical exaggeration. Nonetheless, the restored profile balances, helping us quantify and illustrate the magnitude of gravity-driven salt-related deformation and overburden translation through time.

4 - Base-salt structures

The base-salt surface dips regionally to the SE, with a mean dip of 2º (Figure 4a,b). Local changes in dip angle and direction define base-salt ramps (Figure 4c). In plan-view, these ramps trend NE, broadly subparallel to the margin, are locally concave- or convex-seaward, and are c. 20-180 km long and c. 3-20 km wide. The main belt of base-salt ramps define the boundary between the External High and the External Low (Figures 2 and 4b,c). These ramps have a maximum structural relief of c. 900 ms TWT (c. 2 km) and they dip seaward c. 3º-9º (Figure 4c). The heights of the ramps are thus consistent we those previously reported from the Campos Basin (1.4-1.6 km – figure 24 in Dooley et al., 2017; figure 6 in Davison et al., 2012).
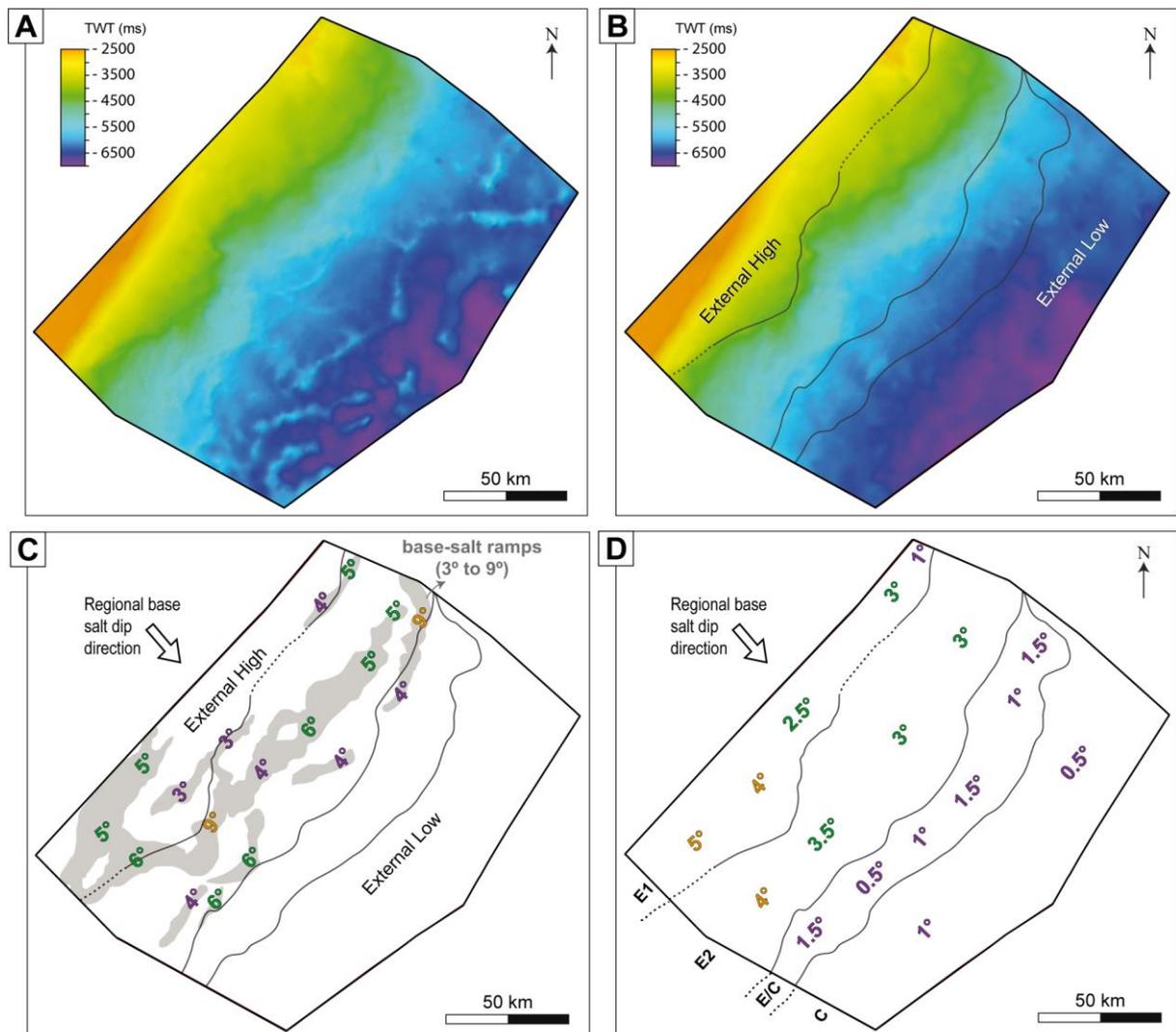

Figure 4. Time maps of the base-salt surface before (A) and after (B) the pull-up correction, showing doming dip to SE. (C) Mapped base-salt ramps shown in grey and their dip angles; the ramps are broadly subparallel to the margin, but with variable geometry along strike. The dip angles are plotted where they were calculated; they vary from 3º to 9º. (D) Average base-salt dip angles in different regions of each domain of deformation (shown in Figure 5).

5 – Structural style of the salt and its overburden

The salt structures interpreted from the salt isochron map (Figure 5) present varying geometries and structural styles. Most structures trend broadly NE, sub-parallel to the underlying pre-salt, rift-related ramps (Figure 5c). Exceptions to this occur in the SW of the study area, where salt-rollers trend N, and in the northeast, where a single E-trending salt wall is found. Salt structures are flanked by apparent primary welds or areas of relatively thin, depleted salt; in these regions, sub-salt and supra-salt strata appear to be in direct contact (white areas in Figure 5a).

Key overburden structures are displayed on the Top Salt to Top Cretaceous isochron map (Figure 6). These structures have broadly the same orientation as underlying salt structures (see detailed descriptions below), and where the underlying salt has pierced the entire Cretaceous succession the latter is absent (white areas in Figure 6a,b). The types, dimensions, and interpreted origins of the salt and overburden structures are summarized in Tables 1 and 2, respectively. We now present the distribution of these structures, which define the three main domains of thin-skinned, salt-detached deformation: extensional, contractional, and multiphase.

5.1. Extensional domain (E)

5.1.1. Description

The extensional domain trends NW and corresponds to nearly half of the study area, with a minimum average width of c. 77 km (Figure 5). All the major base-salt ramps described above occur within this domain, which results in relatively high average values of base-salt dip (c. 2.5°-4.5°) that increase south-westwards (Figure 4d). The base-salt dips increases south-westwards because, even though they maintain the same average dip, they become wider and/or more numerous (Figure 4c). Seaward (i.e. south-eastwards) changes in salt and overburden structures within the extensional domain define two subdomains: E1 (proximal) and E2 (distal).
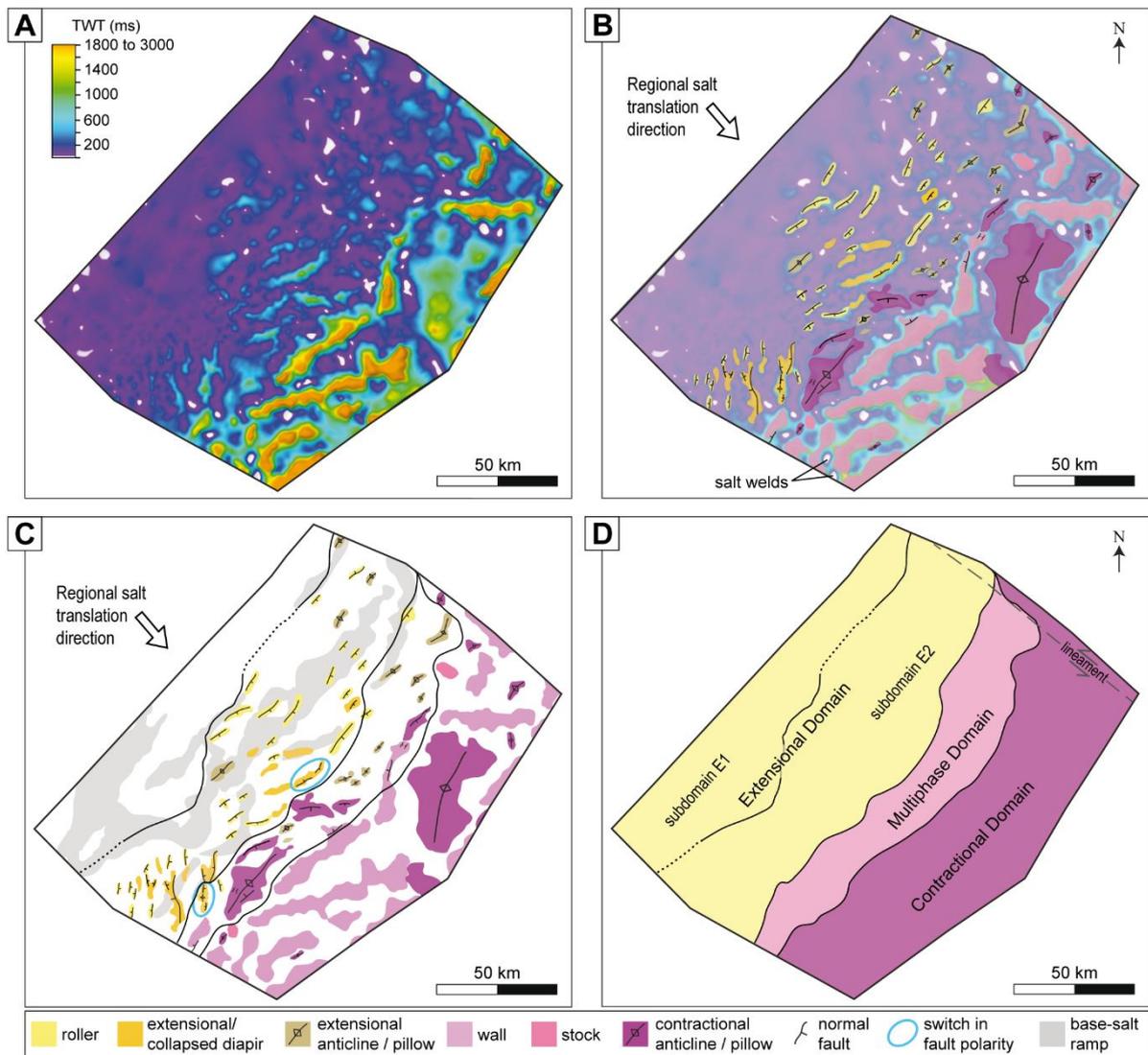
Figure 5. Salt isochron thickness map (A) with the interpreted salt structures in (B); areas of minimal thickness shown in white represent regions where salt is completely to incompletely welded. (C) Distribution of the salt structures across the study area, with the location of base-salt ramps in grey – colours of the structures within the multiphase domain follow their primary deformation. (D) Location of the domains of thin-skinned deformation; the boundary between E1 and E2 is partially dotted due to the scarcity of seismic lines in this region.

Subdomain E1 defines the proximal, upslope portion of the extensional domain. In E1 the salt is relatively thin (0-300 ms, with an average of 80 ms), with limited top-salt relief and thickness variations (Figures 5, 6 and 7). To the southwest, we observe small (200 to 300 ms high) salt rollers bounded by seaward-dipping, salt-detached normal faults (Table 1, Figure 7d,e,f), and tilted raft-like blocks of Albian strata (Table 2). Where salt rollers are absent, for example along-strike to the northeast, salt is largely depleted (<50 ms) to (apparently) welded, or it forms small pillows (Figure 7a,b). The mean base-salt dip is 3º seaward, locally reaching 6º on well-defined, NE-trending ramps (Figures 4c,d and 8).

Subdomain E2 occurs immediately downdip of E1. Salt thickness varies from 0-1450 ms, and numerous elongate, NE-to-N-trending structures are visible on the salt thickness map (Figure 5). The average base-salt dip is 3º, with NE-trending base-salt ramps dipping up to 9º, defining linear to locally concave- or convex-seaward geometries (Figures 4c,d and 8). The key salt and overburden structures in E2 are: (a) salt rollers and their associated salt-detached growth faults/rollover systems, which can laterally pass into RSBs or extensional turtle structures; and (b) collapsed diapirs overlain by grabens and half-grabens (Tables 1 and 2; Figure 7).
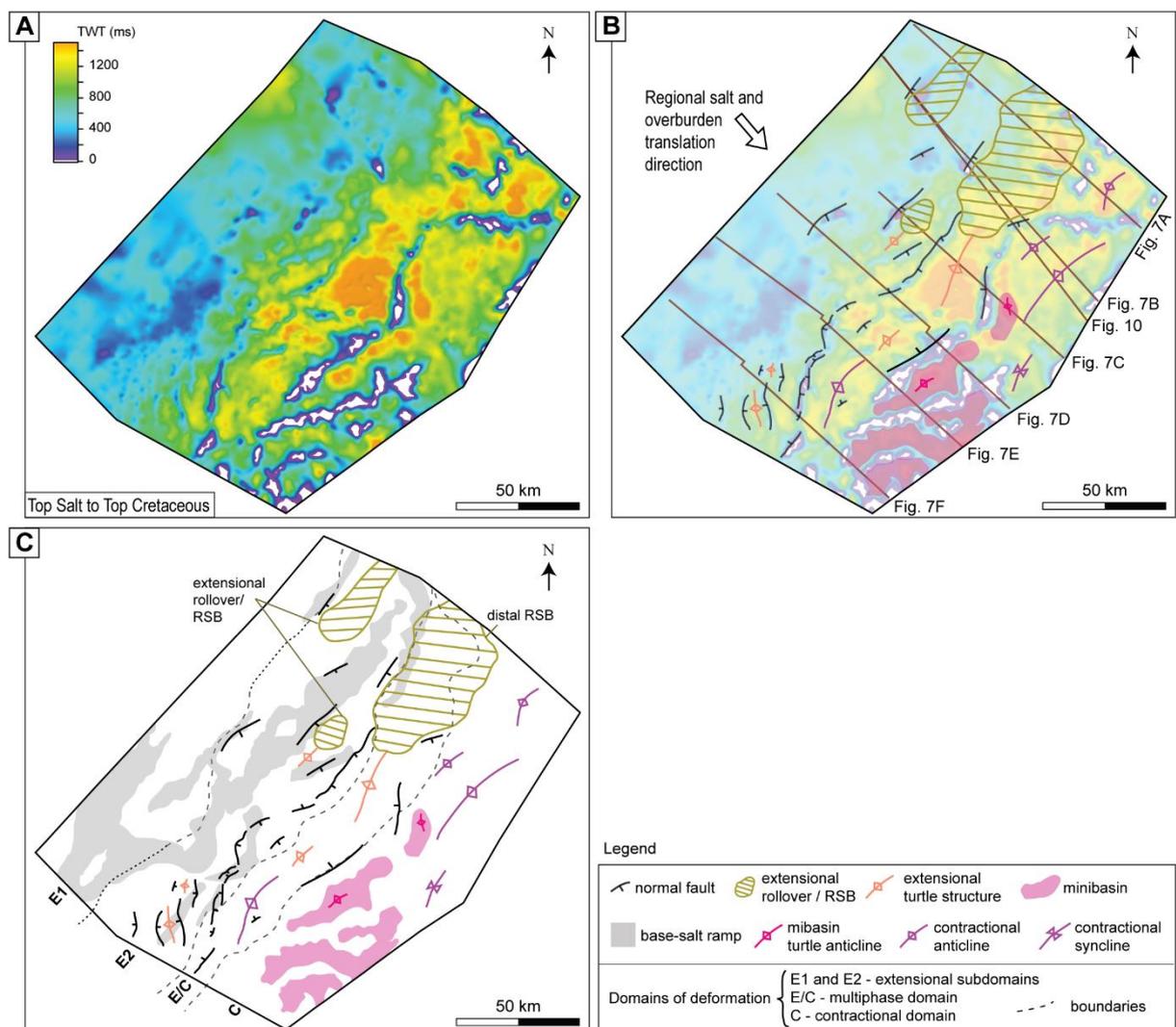

Figure 6. (A) Isochron thickness map from the Top Salt to the Top Cretaceous horizon. (B) Interpreted overburden structures related to salt tectonics onto the isochron thickness map of 6A; this map also shows the location of the seismic lines of figures 7 (and 8) and 10. (C) Distribution of the interpreted overburden structures in 6B, with base-salt ramps in gray and the domains of thin-skinned deformation.

In the NE portion of the study area, salt rollers and extensional rollovers dominate, and these can pass laterally into RSBs (Figure 6; Figure 7a,b) that are locally underlain by extensional anticlines or pillows (Figure 7a -structures 1; Figure 7b - structure 1). The central and south-western regions of the study area are characterized by salt rollers bounded by seaward- or landward-dipping growth faults and flanking rollover systems (Figure 7c to f); these structures occasionally define extensional turtle structures (Figure 7c - structure 2; Figure 7d - structure 2) or grabens above extensionally collapsed diapirs (Figure 7d - structure 3, Figure 7f - structures 1 and 2). There are also more complex extensional diapirs that may have grown from lower-relief rollers in response to periodic switches in the polarity of their bounding faults (see *flip-flop salt walls* of Quirk et al., 2012; extensional diapir in Figure 9, inactive fault segment indicated by a white line near the diapir pedestal). Switches in fault polarity across extensional salt walls can be observed in the salt structure map (Figure 5c - blue ellipses). Salt rollers occur close to or above base-salt ramps (Figure 7d,e,f), whereas collapsed diapirs and grabens tend to overlie areas where the base-salt is flatter (Figure 7d,f). The extensional turtle structures are wider and longer in the central region in comparison to the north-eastern and south-western regions, where the growth faults are also longer (Figure 6b,c). The extensional turtle structures are associated with Cenomanian to Maastrichtian growth strata, and they are cored by salt anticlines or pillows (Figure 7d - structure 2; Figure 9), or folded Albian strata above welded salt (Figure 7c - structure 2). The salt-detached normal faults bounding salt rollers, or those flanking graben formed above collapsed diapirs, are associated with Albian to mid-Neogene growth strata (Table 2 and Figure 7).

5.1.2. Interpretation

The structures within the extensional domain vary along dip, defining the two previously described subdomains (E1 and E2), and along strike. According to Fort et al. (2004), the types of extensional structures formed during salt-detached gliding reflect variations in the strain rate within the ductile salt layer, with the strain rate being mainly controlled by the basal

slope angle (i.e. the local dip of the base-salt surface). Relatively steep and gentle base-salt angles are associated with relatively high and low ductile strain rates, respectively. Fort et al. (2004) demonstrate that salt rollers form on steeper basal slopes, whereas diapirs dominate on gentler slopes. This general model appears to apply to the Campos Basin, with salt rollers overlying base-salt ramps in both subdomains (i.e. in E1 in the central and south-western parts of the study area, and in E2 along-strike of the entire studied part of the margin). The specific length and steepness of the these ramps also appeared to control the specific type of overburden structure that formed, i.e., narrow and steep base-salt ramps in the north-eastern portion of the study area favoured the formation of extensional rollovers/RSBs (Figures 7 and 8 a,b,c), whereas wider ramps in the central and south-western parts of the study area favoured the formation of rollovers that pass laterally into extensional turtle structures (Figures 7 and 8 c-f).
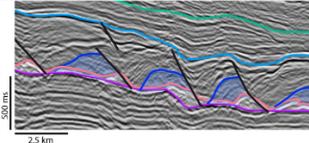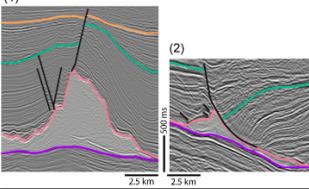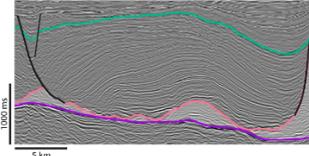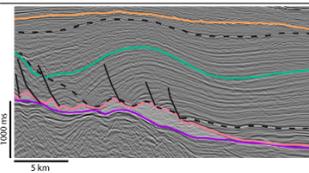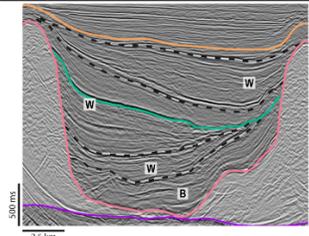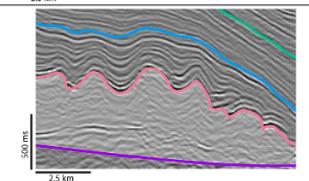
In contrast, areas characterised by gentler base-salt angles are associated with extensional diapirs, that may ultimately widen and collapse with ongoing stretching (Fort et al., 2004 - see their figure 7). Such structural styles are seen in the centre and SW of our study area, where collapsed diapirs tend to develop away from base-salt ramps, on shallower basal slope angles (Figure 7 and 8 d,e,f), and often in association with extensional turtle structures (Figures 7d - structure 2, Figure 9 - west end of the lines). In summary, we suggest that subdomain E1 corresponds to the *sealed tilted blocks* subdomain of Fort et al. (2004), and E2 is at the transition between the *growth fault and rollover systems* and *extensional diapirs* subdomains.

Finally, the formation of RSBs is conventionally defined as a product of translation of salt and its overburden across major base-salt ramps (Table 2) (e.g. Jackson and Hudec, 2005, 2017; Pichel et al., 2018). The RSBs in the extensional domain here are slightly unusual in that they form along-strike of extensional rollovers (Figure 7a - structure 1, 7b - structure 1; Figure 10), which means that translation of salt and its overburden downdip is partially accommodated by the coeval formation of and slip on, salt-detached faults (Evans et al., 2021).

Table 1. Salt structures, their description, dimensions and genetic interpretation.

Structure	Example	Description (e.g. geometry, distribution, and overburden seismic-stratigraphy)	Dimension	Genetic Interpretation
Extensional salt rollers		Relatively narrow, low-relief salt diapirs, bound on at least one side by a salt-detached normal fault (see Table 2). Strata in the footwall of this fault are up-turned and concordant with top salt; in the hanging wall, strata are in faulted contact with the salt. In upslope positions (Type 1 rollers; see column to right) they are relatively small, typically underlying and separating rafts (Table 2), and may be separated by primary welds; in downslope positions (Type 2 rollers; see column to right) they occur next to landward- or seaward-dipping salt-detached normal faults and associated extensional turtle structures (Table 2) or rollover systems. In toe-of-slope positions, salt rollers can also occur on top of salt anticlines.	(1) 1–2 km wide; up to 200 ms TWT high. (2) 4.7–20 km long; 1.5–5.5 km wide; up to 600 ms TWT high.	In upslope positions the seaward flow of salt drives overburden extension, which is accommodated by normal faulting. Differential loading of salt drives reactive diapirism and the formation of salt rollers that rise into the immediate hangingwall of salt-detached faults. In toe-of-slope positions, in the multiphase domain, later extension and faulting of salt contractional anticlines locally drove reactive rise and the formation of salt rollers. *Source*: Fort et al. (2004); Brun and Mauduit (2009); Jackson and Hudec (2017).
Extensional/ collapsed diapiric salt walls		Triangular-shaped diapirs defined by wide bases and narrow crests. They are located in downslope positins, adjacent to Type 2 rollers. Diapirs are flanked and overlain by small, inward-dipping, salt-detached normal faults (Table 2). Flanking strata onlap or downlap onto, and often upturned against, top salt. Diapir crests are either rounded or U-/V-shaped; in the latter case, the shape arises due to the presence of horn-link cusps located in the hangingwall of overlying crestal faults (cf. salt rollers). The size and orientations of the faults vary, but they typically define crestal grabens filled with growth strata.	5.3–12.3 km long; 1.4–5 km wide; up to 1300 ms TWT high.	Thin-skinned extension of the overburden causes normal faulting and the formation of grabens and half-grabens. Differential loading of underling salt drives reactive diapirism and salt wall formation. Continuing extension may cause diapirs to widen until the salt source layer becomes depleted and/or strongly restricted; diapir crests then begin to sag, driving normal faulting of and graben formation in overburden rocks. *Source*: Vendeville and Jackson (1992a,b).
Salt anticlines and pillows		Convex-up bodies of salt that have a concordant (i.e. non-diapiric) contacts with overburden strata. These structures occur across the entire study area; their dimensions increase towards the the downdip end. In downslope positions these structures are the core of extensional turtle structures (Table 2). Overburden commonly faulted (salt-detached normal faults - Table 2) and folded (extensional anticlines and contractional folds - Table 2).	*extensional*: up to 15.8 km long up to 3.5 km wide up to 450 ms TWT high *contractional* 5.5–50.8 km long; 2.7–27 km wide; up to 1800 TWT ms high; λ = 10–25 km	Depending on their plan-view length-to-width ratio, these salt bodies are called pillows (ratio <2) or anticlines (ratio >2). In downslope they are associated to extensional turtle structures (Table 2), originated by thin-skinned extension (extensional salt anticlines and pillows). At the toe of slope and towards the downdip end of the study area, the structure form due to overburden shortening and salt inflation immediately seaward of base-salt ramps due to a salt flux imbalance associated with thickness variations of the salt layer (contractional salt anticlines and pillows). *Source*: Dooley et al. (2017) and (2018); Jackson and Hudec (2017).
Diapiric salt walls and stocks		Triangular to columnar salt structures in cross-section, characterised by discordant (i.e. diapiric) contacts with their overburden. In map-view these bodies are either sub-circular or elongated, located downdip the toe of slope. Often capped by an arched and faulted roof. High-relief structures underlie relief at the present seafloor. Commonly flanked by upturned megaflaps (sensu Rowan et al., 2016) of overburden strata which can be partially eroded by exposure (see example 2).	*stocks*: up to 10 km long; up to 5.3 km wide; up to 1500 ms TWT high. *walls*: 14–72 km long; 2.2–14.4 km wide; up to 3000 ms TWT high.	Salt diapirs can grow via a range of mixed processes. Those in the contractional domain record mainly two mechanisms of diapiric rise: (a) passive diapirism, associated with syndepositional downbuilding of flanking diapirs); and (b) active diapirism, caused by regional thin-skinned compression, which also leads to overburden arching and faulting. Megaflaps may record a preceding stage of salt inflation and formation of a pillow or anticline, which was then broken through by a growing diapir. *Source*: Rowan et al. (2016); Jackson and Hudec (2017).

Table 2. Salt-related overburden structures, their description, dimensions and genetic interpretation.

Structures	Example	Description	Dimension	Age of Growth Strata	Genetic Interpretation
Rafts		Rotated blocks (rafts) of overburden strata bound by salt-detached normal faults, separated by salt rollers and/or trough-like deposits of younger, synkinematic strata (see Table 1). Typically underlain by salt welds. Rafts occur updip in the study area.	2–3.2 km wide; 200–300 ms TWT high.	Early to mid-Albian.	Formed due to extensional dismemberment of overburden strata during gravity gliding. Synkinematic depocentres form between rafts. *Source*: Quirk et al. (2012); Jackson and Hudec (2017).
Salt-detached normal faults		Overburden-restricted normal faults that detach within salt. Bound salt rollers and associated rollover systems (example 2) and rafts, and can displace overburden strata capping the crests of salt anticlines (example 1) and as well as various types of diapirs (Table 1). May offset strata filling ramp-syncline basins. The faults dip landward- or seaward-, and are either listric or planar in cross-section.	up to 37 km long; up to 750 ms TWT of vertical throw.	*subdomain E1*: Albian; *subdomain E2*: Albian–mid-Neogene; *E/C Domain*: Albian–mid-Neogene; *Cont. Domain*: Albian–Recent.	Salt-detached normal faults accommodate thin-skinned extension of overburden. They can form: (i) in the proximal domains (ie. E1 and 2) due to the seaward flow of salt and associated overburden stretching; (ii) in the distal domain (i.e. C domain) due to outer-arc bending-related stretching of overburden above salt pillows and anticlines; (iii) due to overburden stretching above extensionally collapsing diapirs. *Source*: Fort et al. (2004); Jackson and Hudec (2017).
Extensional turtle structures		Anticlines bounded by oppositely and inward-dipping, salt-detached normal faults that also bound salt rollers and walls. Anticlines cored by salt pillows and anticlines (Table 1). Anticline-related growth strata are asymmetric, thickening towards one or both flanking faults. In map-view, the these anticlines are elongated and trend parallel to their bounding normal faults.	up to 32.1 km long; up to 30 km wide; up to 1500 ms TWT high.	Albian–Early Paleogene.	Salt-detached normal faults with opposite dips are generated by thin-skinned extension. Salt flow into fault footwalls causing local overburden collapse, and ultimately the formation of a salt-cored anticline called a 'turtle'. *Source*: Lundin (1992); Quirk et al. (2012).
Ramp syncline basins		Synclinal basins located in the hanging-wall of salt-detached normal faults and associated rollover systems. Typically located above and slightly seaward of seaward-dipping base-salt ramps. RSB growth strata dip and thicken landward, defining a monoclinal geometry. Downdip, the detachment surface (lower black dotted line) is marked by strata onlap or apparent downlap.	16–63.7 km long; 10–35 km of translation.	Albian–mid-Paleogene.	RSBs that form in response to the downdip translation of salt and its overburden across major base-salt ramps. The lateral distance between the top of the ramp and the seaward-most onlap (or apparent downlap) termination defines the magnitude of translation. *Source*: Jackson and Hudec (2005); Jackson and Hudec (2017).
Minibasins		Synclinal depocentres bounded by thick, diapiric salt. Depocentre strata thin towards and onlap onto bounding diapirs. Basal depocentre strata are symmetric, defining "bowl-shaped" geometries (B); these can be overlain by more asymmetric wedges of strata (W) thicken towards onto of the bounding diapirs. Basal megaflaps are common. Depocentres are floored by salt or a primary weld. Locally, multi-wavelength folds are developed within basal strata. In map-view, these depocentres are elongated parallel to bounding salt walls. Depocentres can be isolated or partially connected.	amplitude: 35–110 ms TWT and up to 1500 ms TWT λ = 0.5–2.5 km and 10–25 km	Albian–Top Paleogene.	Minibasins formed by density-driven subsidence of overburden into underlying salt. Subsidence may occur during lateral shortening. Bowl-shaped stratal packages (B) record symmetrical subsidence, whereas wedge-shaped pacakges (W) record asymmetric subsidence and minibasin tilting. Abrupt shifts in wedge depocentre location may reflect syn-subsidence shortening, which causes one bounding diapir to inflate more rapidly than the other. *Source*: Jackson and Hudec (2017); Jackson et al. (2019).
Contractional folds		Convex-up bodies, typically polyharmonic, with multiwavelength growth composed by early high-frequency folds and a larger wavelength growth. There can be faults dissecting the crest of the antiforms.	25–52.3 km long; 4.3–17 km wide; up to 1500 ms TWT deep.	Early Albian–Early Neogene.	High frequency folds formed when the overburden was thin, due to shortening immediately seaward of base-salt ramps in response to a salt flux imbalance associated with thickness variations of the salt layer. Subsequent regional thin-skinned compression promoted fold growth in larger wavelength. *Source*: Cobbold and Szatmari, (1991); Fort et al. (2004)

5.2. Contractional domain (C)

5.2.1. <u>Description</u>

The contractional domain defines the downslope portion of the study area. This domain trends NE and has an average width of c. 39 km, being widest in the NE where it is up to 75 km wide, just to the north of a NW-trending, basement-involved lineament (Figure 5d). Base-salt is smoother in the contractional domain than in the extensional domain, with the mean seaward dip varying from 0.5º to 1º (Figure 4d). Salt is thickest in this domain (up to 3000 ms), being arranged into NE-to-E-trending broad salt anticlines underlying buckle folds, and salt walls and stocks (Table 1 and Figure 5) that are flanked by minibasins (Table 2 and Figure 6b,c).

One of the most prominent structures within the contractional domain is a large, salt-detached fold belt (51 km long and up to 27 km wide; Figure 5), comprising stacked, multiwavelength folds, i.e., relatively short-wavelength (0.5-2.5 km) and low-amplitude (35-110 ms) folds at top salt pass upwards into longer wavelength (10-25 km) and higher-amplitude (up to 650 ms) folds in the overburden (Figure 7b - structure 4; Figure 7c - structure 5). Similar structures are described by Davison et al. (1996), Demercian et al. (1993), Dooley et al. (2017) and Erdi and Jackson (2021).

Diapiric structures, commonly salt walls, predominate in the contractional domain (Figure 5c). These structures are up to 72 km long and 14 km wide, and are triangular to columnar shaped in cross-section (Table 1). The diapirs are often capped by an arched or uplifted roof (Figure 7a - structure 3, 7b - structure 5, 7d - structure 7, 7e - structure 5, 7f - structure 3). Upturned megaflaps (*sensu* Rowan et al., 2016), frequently topped by erosional truncations flanking one side of the diapirs, are also common (Figure 7a - structure 3, 7e - structure 8, 7f - structures 3 to SE and 6), and they are sometimes ornamented by now-rotated and uplifted trains of the high-frequency buckle folds described above (Figure 7d - structure 7).

Post-salt Cretaceous overburden is thin to absent over salt walls in the contractional domain, but is very thick (up to 1800 ms) in the flanking minibasins (Figures 6 and 7d,e,f). Minibasins occur in the centre and SW portions of the study area (Figure 6c), where they are overall symmetric (Figure 7e - structures 6) or asymmetric (Figure 7d – structure 6) and are floored by salt (Figure 7f - structures 4) or primary welds (Figure 7f - structure 5). The minibasins can sometimes assume an antiformal, turtle-like shape (Figure 7c - structure 4).

5.2.2. Interpretation

We interpret that the high-frequency buckle folds formed by thin-skinned shortening when the overburden is thin (Cobbold and Szatmari, 1991; Fort et al., 2004; Dooley et al., 2017), meaning contraction started soon after salt deposition (i.e. during the earliest Albian; cf. Demercian et al., 1993; Quirk et al., 2012 - Figure 1c). Early, short-wavelength folds at the base of the polyharmonic folds form when the overburden is thin, either by local variations in salt flux across a seaward-dipping ramp (Dooley et al., 2017), or by regional shortening (Fort et al., 2004). After the formation of these early folds, the strength of the folded layer increases in response to synkinematic sedimentation, resulting in a progressive increase of fold wavelength (Cobbold and Szatmari, 1991; Fort et al., 2004). Shortening then becomes concentrated within the growing anticlines, trapping and pinching salt within the anticlinal cores and leading to the generation of contractional diapirs (see Figure 7d - structures 7 and 8) (Fort et al., 2004; Rowan et al., 2016 – see their figure 13). Shortening-driven active rise of these diapirs resulted in the uplift and outward-tilting of the flanking megaflaps and arching of their roofs (Table 2) (Jackson and Hudec, 2017) Diapirs formed in this way can subsequently rise passively if they reach the free surface (Jackson and Hudec, 2017).

Not all diapiric structures in the study area have geometric or seismic-stratigraphic features diagnostic of their formation due to thin-skinned shortening nor extension, suggesting they largely grew in response to passive diapirism (e.g. Figure 7d - structure 7). However, we

interpret that these structures are kinematically part of the contractional domain given they are spatially associated with contractional structures and were thus likely triggered by (or are associated with) shortening.

Minibasins form primarily by due to subsidence of overburden into underlying salt. This subsidence is load-driven (i.e. overburden sinks and salt is expelled laterally), recorded by the deposition of bowl-shaped, symmetrical packages, or wedge-shaped, asymmetrical packages of sedimentary strata (Table 2). Abrupt shifts in the wedges depocentres locations (Figure 7e - structure 6a; 7f - structure 5; Table 2) may reflect coeval lateral shortening, which causes one bounding diapir to inflate more rapidly than the other (Jackson et al., 2019). Turtle anticlines within minibasins (Figure 7c - structure 4) originate due to partial or full depocentre inversion caused by minibasin welding at the minibasin centres, and the onset of subsidence and salt expulsion at their flanks (Trusheim, 1960; Peel, 2014).

5.3. Multiphase domain (E/C)

5.3.1. Description

This domain is located between the extensional and contractional domains, presently located at the toe of the ramp between the External High and External Low. The domain has a mean width of 25 km (Figure 5) and base-salt has average seaward dip of 0.5º to 1.5º (Figure 4d). Salt thickness in the multiphase domain ranges from 0-2100 ms, commonly composing NE-trending, irregular to elongated structures, and more rarely, N- and E-trending structures (Figure 5).

In the NE, this domain is fundamentally translational (or transitional), characterized by a large ramp syncline basin (RSB) (Figure 6c) that is locally associated with salt rollers of subdomain E2 (Figure 7b - structure 2, 7c - structure 1; Figure 10). Along-strike to the

21

southwest, the multiphase domain is characterized by three types of salt structures with a hybrid extensional-contractional evolution. The most common type consists of contractional anticlines, which were subjected to later extension and normal faulting (Figure 7d - structure 4) that locally drove reactive rise and formation of salt rollers (Figure 9 - structure 2) and overlying grabens (Figure 7b - structure 3). The second most frequent type of structure comprises diapirs with passive and active growth histories, and which are overlain and partly flanked by landward-dipping normal faults that displace the diapir roof (Figure 7c - structure 3; Figure 7d - structure 5) and that may bound extensional turtle structures (Figure 7c - structure 3). Lastly, we observe an extensional diapir that was subsequently squeezed, with the latter phase of active diapirism driving arching and normal faulting of the diapir roof (Figure 9b - structure 1) or folding and uplift of strata above the collapsed diapir graben (Figures 9c – structure 3, and 7f - structure 2, between the Top Cretaceous and Top Paleogene).

5.3.2. Interpretation

Like the smaller RSBs in the extensional domain, the large RSB in the multiphase domain records horizontal translation, which is partially accommodated by the formation of salt-detached faults (Figure 7b - structure 2, 7c - structure 1; Figure 10). The balanced kinematic model in Figure 10 shows the hybrid origin of these structures (see also section 6).

The contractional anticlines that were subjected to later extension and normal faulting of the multiphase domain have two alternative origins. The first is that salt and its overburden translated across two seaward-dipping, base-salt ramps, with an anticline initially forming across the contractional hinge of the first ramp, before this fold was subsequently extended above the extensional hinge of the second. Schematic illustrations in Figure 10f,g elucidate this mechanism. During the early Albian, salt flow across the updip base-salt ramp caused active salt upwelling across the contractional hinge at its base, folding the prekinematic strata (Figure 10g – structures 5 and 6). Further translation across the downdip ramp reactivated the antiform

in response to extension, generating two normal faults and triggering reactive diapirism (Figure 10f – structure 5). This multiphase deformation mechanism may also be applied to smaller structures in this domain (Figures 5c, 7b - structure 3, 7d - structure 4), which record deformation ceasing by the end of the Cretaceous (Figure 10 – structure 5). Complex salt structure with a similar origin and evolution are documented in the Kwanza Basin, offshore Angola (Erdi and Jackson, 2021 – see their figure 9b), in the Santos Basin, offshore Brazil (Pichel et al., 2019a), and from numerical models (Pichel et al., 2019b).

The second origin for the formation of contractional anticlines that were subjected to later extension is the seaward migration of extension through time, resulting in extensional inversion of previously contractional structures (Brun and Fort, 2011). Downdip migration of extension occurs after grounding of updip structures due to salt welding and/or margin progradation. This model may apply to the largest contractional structure to the SW (Figures 5c, 9 - structure 2). This structure initially grew into a multiwavelength salt anticline during the Albian and Late Cretaceous (see section 5.2.2), and later was extended, locally developing salt rollers as indicated by the presence of salt-detached normal faults associated with Paleogene growth strata (Figure 9 - structure 2). The salt was welded updip of the structure so that the system became pinned further updip whilst the downdip salt anticline was still able to translate and extend. The weld-driven migration of extension may also account for the evolution of diapirs that witnessed phases of active and passive growth, given these structures are associated with relatively young (late Cretaceous – Paleogene) salt-detached normal faults (Figure 7c - structure 3, 7d - structure 5) that likely formed after the adjacent primary welds.

Finally, in the SW of the multiphase domain there is one extensional diapir that underwent later contraction (Figure 9 - structure 1). Differential salt flow along base-salt steps may have caused the later contraction of the extensional diapir. The abundance of magmatic intrusions and intense faulting in the south-west part of the study area (Figures 7e,f, and 9) may also, in some way, have influenced the complex evolution history of this structure.
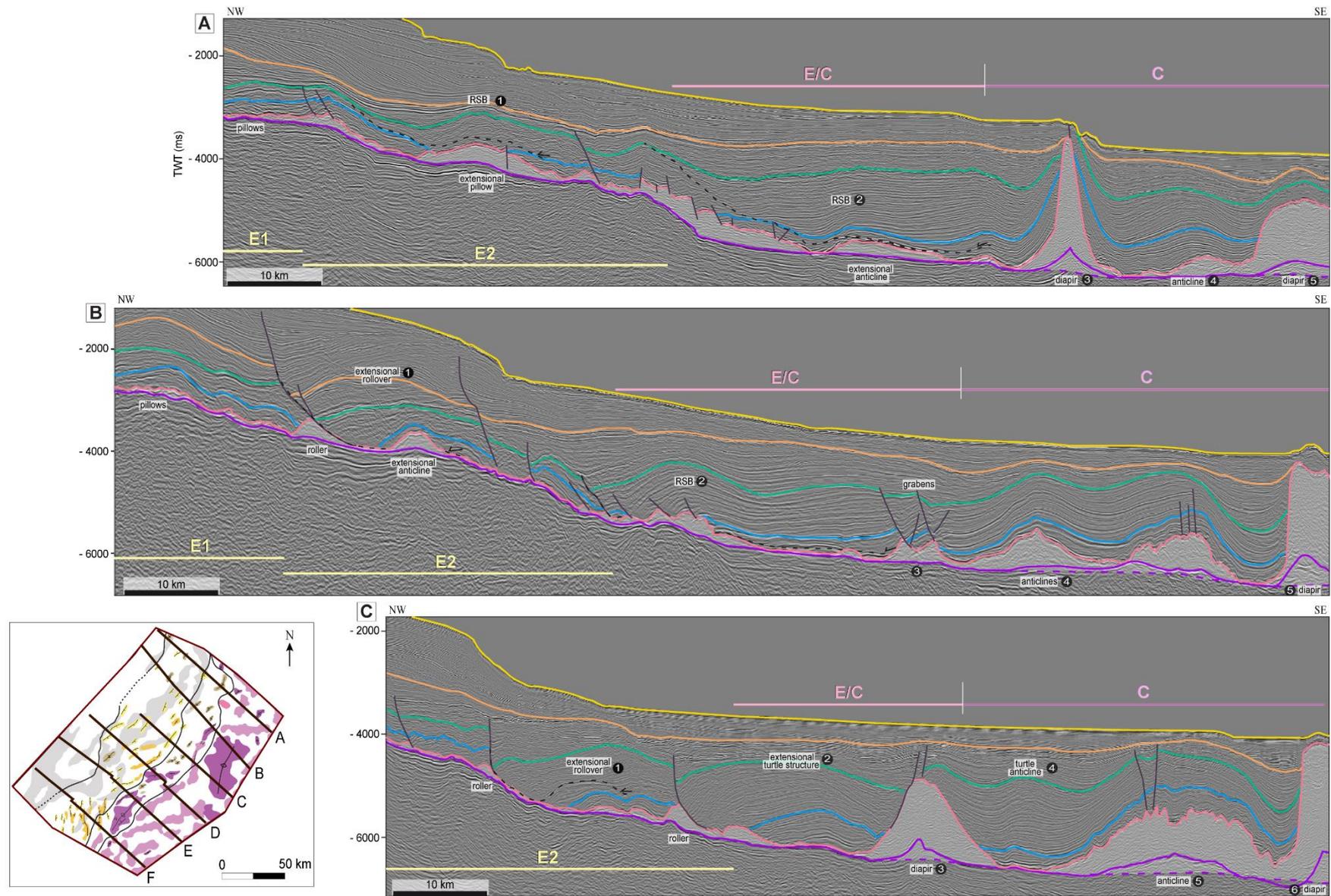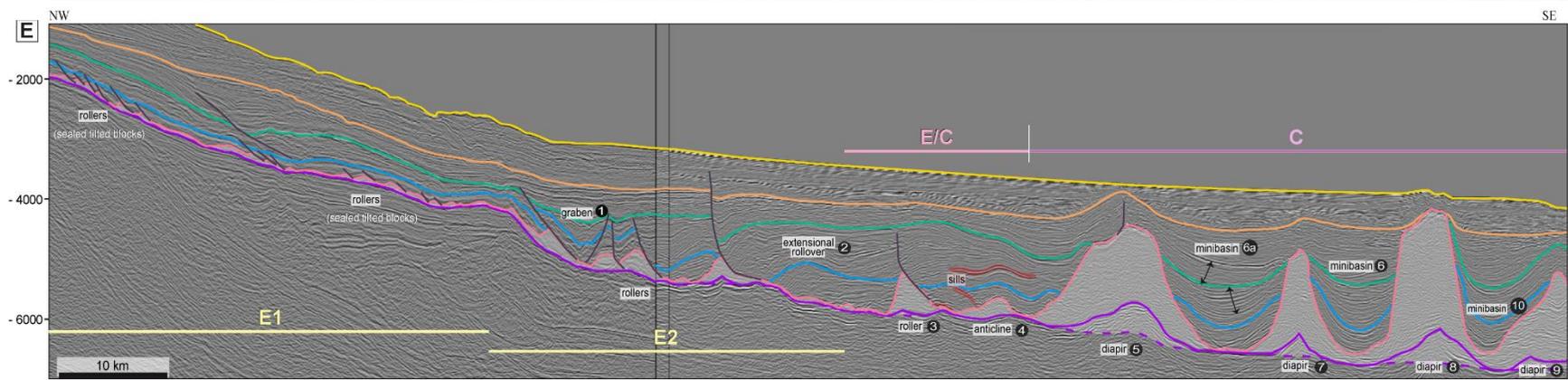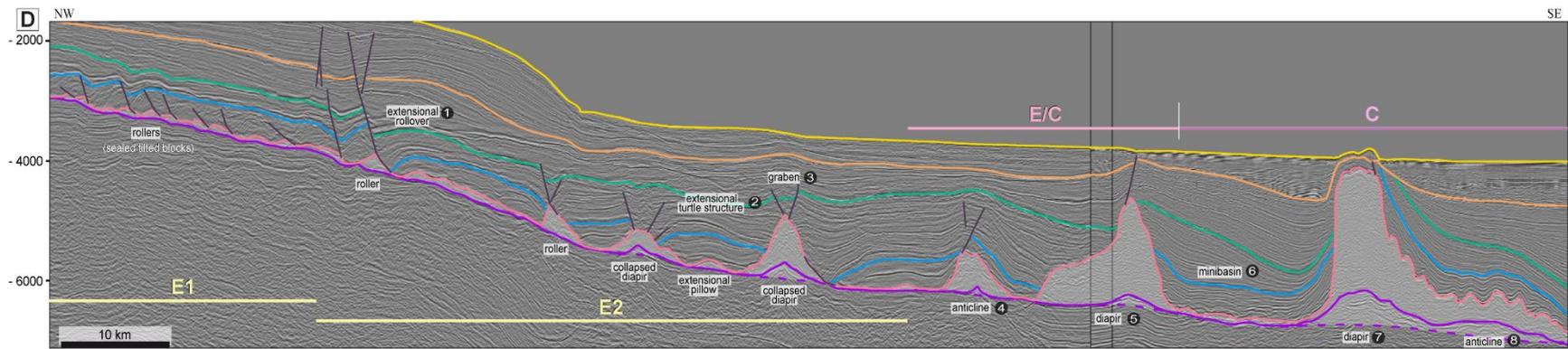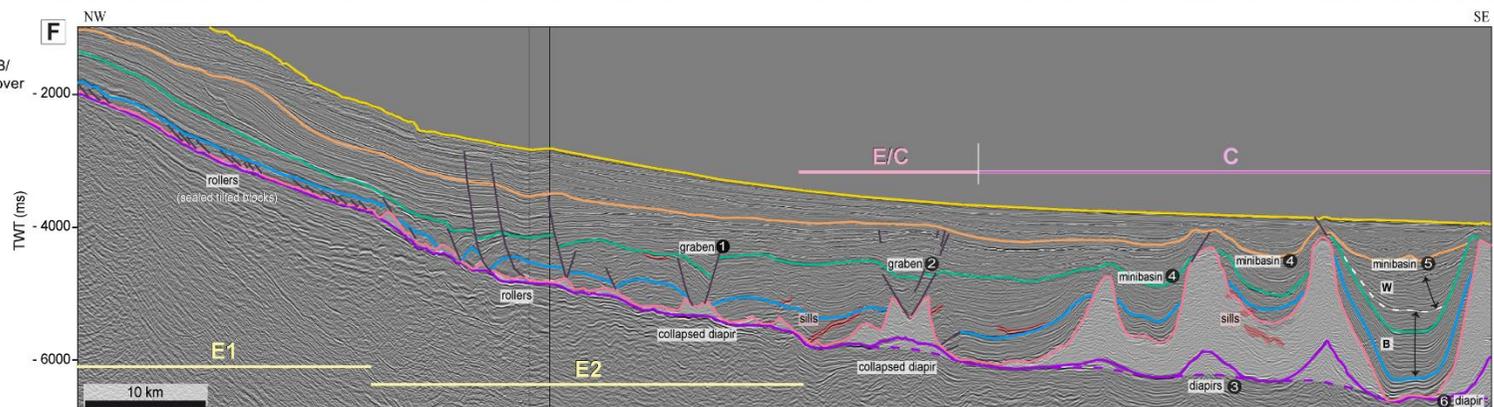
Figure 7. Interpreted dip lines in the north (A), (B), centre (C), (D), and south (E), (F) of the study area, with the interpreted seismic horizons, salt and overburden structures, and domains of deformation; the map left from (C) shows the locations of the lines onto the interpreted salt structures. Salt and overburden structures are numbered to facilitate indications in the text. The dotted white line in (F) represents the shift from bowl-shaped (B) minibasin to wedge-shaped (W). Seismic data supplied by ANP.

6 – Evolution of extensional and contractional deformation through time

Using temporal changes in sediment thickness patterns, seismic-stratigraphic relationships (i.e. onlap, erosional truncation), and balanced structural restorations, we reconstruct the evolution of the study area during three key time intervals: Albian to End-Cretaceous, Paleogene, and Neogene to Recent.

6.1. Albian to Top Cretaceous

Thin-skinned extensional and contractional deformation had already begun during the Albian (and possibly as early as the Aptian; Cobbold and Szatmari, 1991; Fiduk and Rowan, 2012; Davison et al., 2012) as salt began to flow downdip towards the basin. Regional thin-skinned extension of overburden in the proximal subdomain E1 commenced and ceased during the Albian as shown by the occurrence of fault-bound Albian growth strata, with the fault tips sealed by post-Albian strata (Figures 7 and 8d to f). By the late Albian, salt welds had formed, associated with grounding of Albian rafts and the cessation of faulting (Fort et al., 2004). In subdomain E2, extension continued for longer, finishing near the end of the Cretaceous. Salt-detached normal faults and salt rollers formed in the central and southwestern parts of the study area, bounding extensional turtle structures (Figures 7c - structure 2, 8c and 9). Early reactive diapirs formed and subsequently collapsed, with most of this deformation ceasing by the end of the Cretaceous (Figures 7d-f and 8d-f). In the northeast of E2 and in the multiphase domain, extensional rollovers developed, as illustrated by the balanced kinematic model of line 0239-0362 in Figure 10a-e. The salt-detached normal faults bounding the salt rollers formed during the Albian (Figure 10e). As salt and its overburden flowed downdip, the salt-detached faults

continued to slip and grow, continually creating accommodation as recorded by the deposition of packages of syn-kinematic strata that thicken towards the faults (Figure 10d).

Local contractional deformation induced by base-salt relief started in the early Albian, as recorded by the deposition of growth strata flanking high-frequency buckle folds in the contractional (Figures 7b - structure 4, 7c - structure 5, 7d - structures 7 and 8, 10f,g) and multiphase domains (Figures 9 - structure 2, 10f,g). With ongoing translation, early contractional structures that formed at the toe of seaward-dipping base-salt ramp were further shortened and evolved into larger-wavelength salt anticlines (Figure 7b - structure 4, 7c - structure 5, 7d - structure 8; Figure 9 - structure 2; Figure 10 – structure 6). Some of these early contractional structures were subsequently extended and faulted (Figure 7b - structure 3, 7d - structure 4, Figure 9 - structure 2; Figure 10c-f – structure 5), with deformation of these multiphase structures ceasing near the end of the Cretaceous.

Regional thin-skinned contraction also caused active diapirism near the end of the Cretaceous, as recorded by upturned megaflaps topped by erosional truncations (Figures 7a - structure 3, 7d - structure 7, 7f - structure 3 and 8a,d,f). Passive diapirism also occurred during much of this Period, as recorded by stratal thickening into flanking minibasins (e.g. Figure 7e - structure 6, 7f - structure 4). Near the end of the Cretaceous, downdip migration of regional extension led to the development of landward-dipping normal faults against two salt walls, bounding extensional turtle structures (Figures 5c, 7c - structure 2, and 8c).

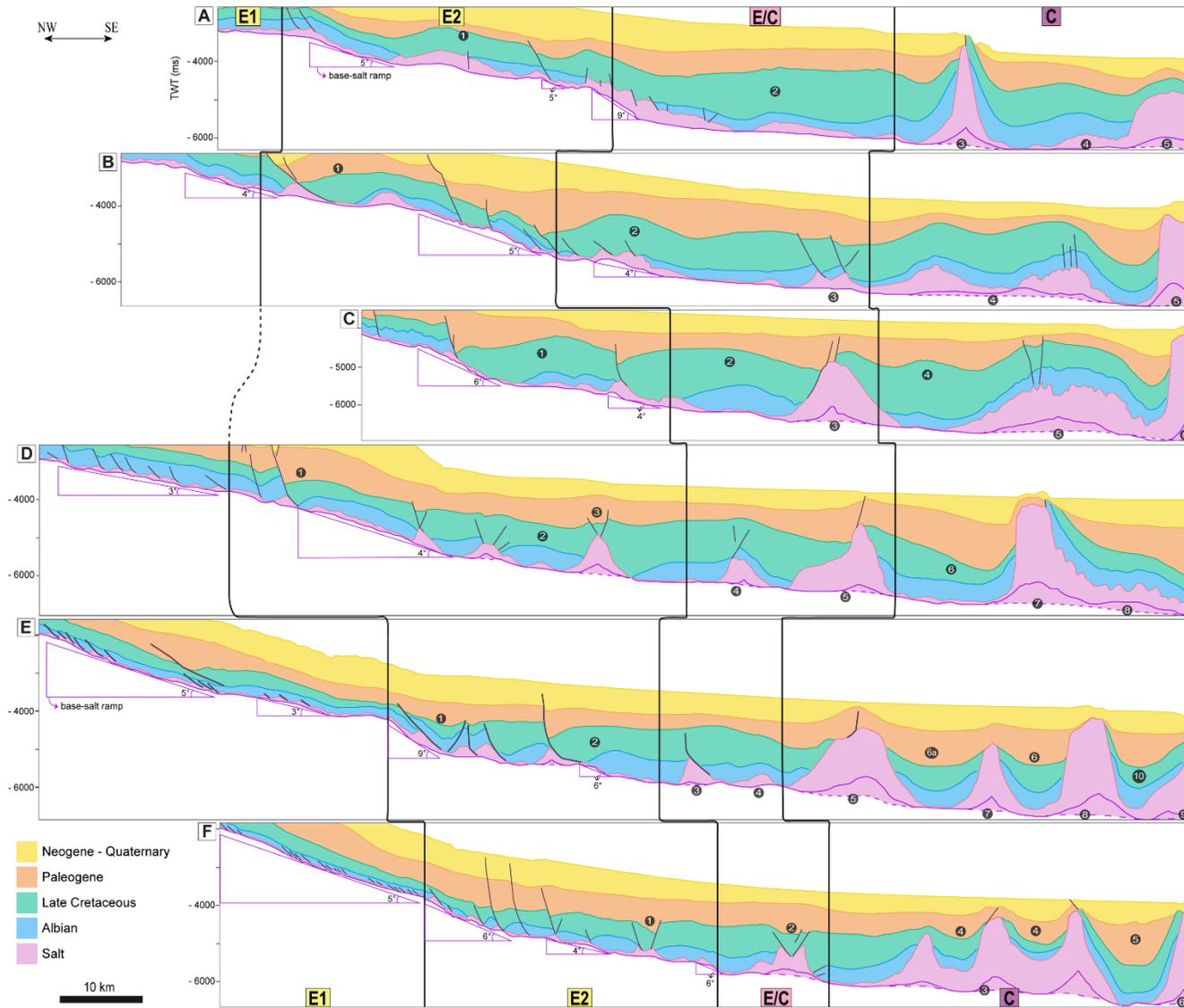**Figure 8.** Stratigraphic intervals of the seismic geosections shown in Figure 7, with the spatial distribution of the deformation domains. The stratigraphic intervals have been coloured to highlight thickening and thinning relationships, indicating timing of the deformation. Base-salt ramps are indicated with triangles, together with their dip angles. Salt and overburden structures are numbered according to Figure 7.

6.2. Paleogene

Regional thin-skinned extension continued through the Paleogene, with faults related to extensional turtle structure formation continuing to slip in subdomain 2 (Figures 7c - structure 2, 8c and 9). Further downdip, in the multiphase domain, an RSB developed in response to further seaward translation of salt and its overburden (Jackson and Hudec, 2005; Pichel et al., 2018) (Figure 10c,b – structure 4). The multiwavelength anticline was extended and faulted because of welding further updip; this extension locally caused the reactive rise of salt and the formation of a roller (Figure 9 - structure 2). Faulted salt walls bounding extensional turtle structures within the multiphase domain accumulated significant throw, becoming inactive by the mid-Paleogene (Figures 7c - structure 2 and 8c).

Regional thin-skinned contraction also occurred throughout the Paleogene. The extensional diapir in the multiphase domain was squeezed at this time, resulting in active rise and folding of its roof (Figure 9 - structure 1). Salt-detached anticlines in the contractional domain were amplified due to ongoing shortening and syn-kinematic sedimentation (Figures 7b – structure 4, 7c- structure 5, 8b,c and 10b,c – structure 6). Diapirs in the contractional domain continued to grow actively and passively, with deepening of flanking minibasins until salt welding (Figures 7d -structure 6, 7f - structure 5 and 8d,f) and folding of their roofs occurred (Figure 7a - structure 5).

6.3. Neogene to Recent

The period between the Neogene to Recent records very little thin-skinned extension, with salt-detached normal faulting being largely inactive by this time (Figures 7 and 8). The seaward flow of salt and overburden continued until the middle Neogene, at least in the area were the hybrid extensional rollover-RSB formed (Figure 6c; Figure 10a,b – structure 4). Anticline growth in the contractional domain ceased in the Miocene (Figure 10a,b –structure 6), whereas active rise of diapirs, presumably due to ongoing horizontal shortening, continued

until recently and may still be ongoing (Figures 7a - structure 3, 7b - structure 5, 7c structure 6, 7d - structure 7 and 8a-d).
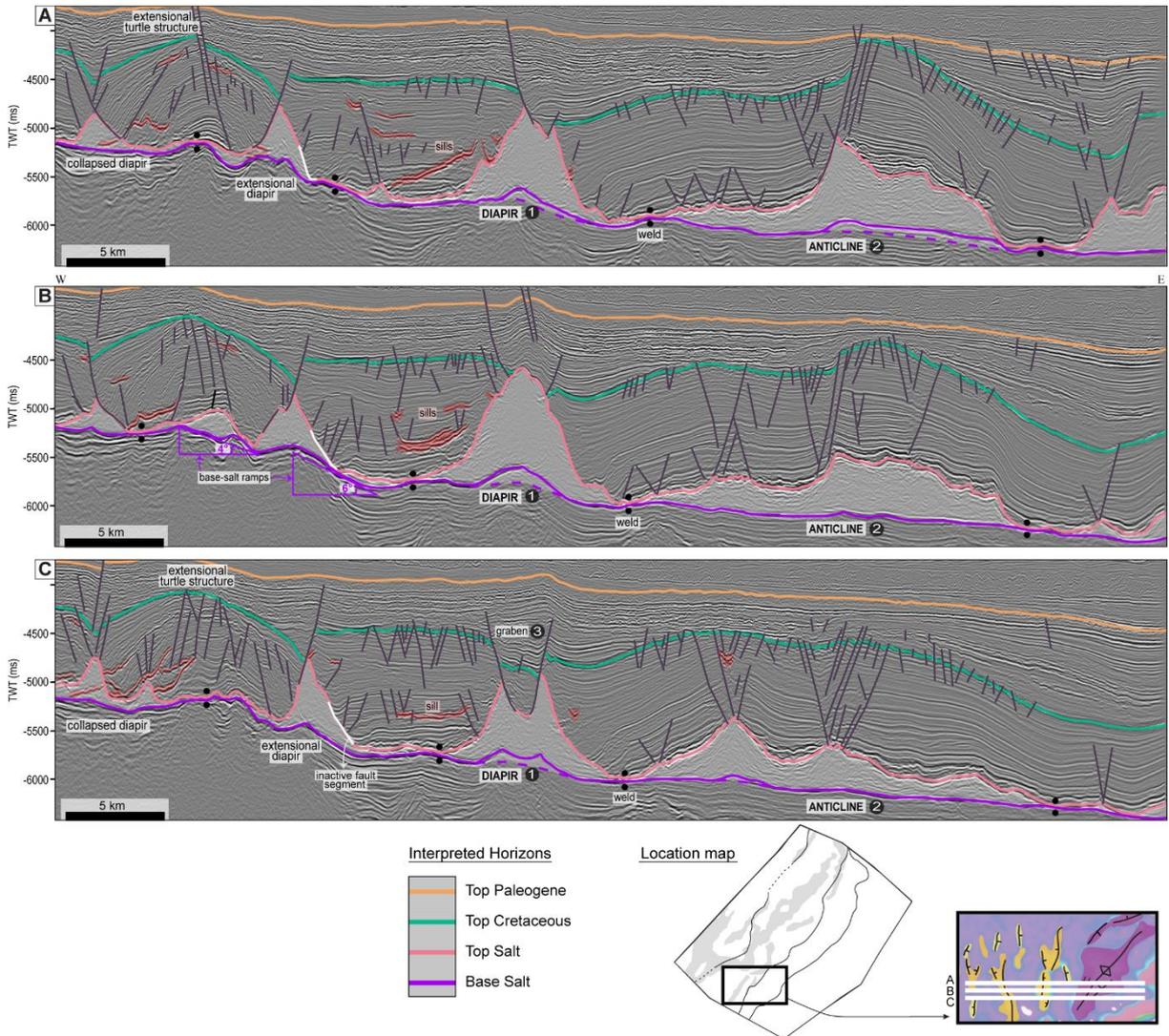
Figure 9. Interpreted seismic inlines of the 3D volume, with the interpreted seismic horizons, labelled salt and overburden structures, and base-salt ramps with their dip angles. (A) is north, (B) centre and (C) south – spacing between the lines is 1.6 km (see map in the bottom right for location). The sections show the boundary between the extensional domain (subdomain E2) and the multiphase domain. Salt and overburden structures are numbered to facilitate indications in the text. Note the abundance of sills and faults. Seismic data supplied by ANP.

Balanced kinematic model

A — NW / SE; extensional rollover ②; roller ①; E/C; C; RSB ④; roller ③; E1; E2; 20 km; multiphase ⑤; anticlines ⑥; TWT (ms)

B — Miocene restored

C — Paleogene restored; 3 km

D — Upper Cretaceous restored; 18 km

E — Upper Albian restored; Lower Albian; 28 km of translation; 19 km of extension; 28 km of translation

Schematic illustrations

F — ⑤ ⑥

G — ⑤ base-salt ramp ⑥
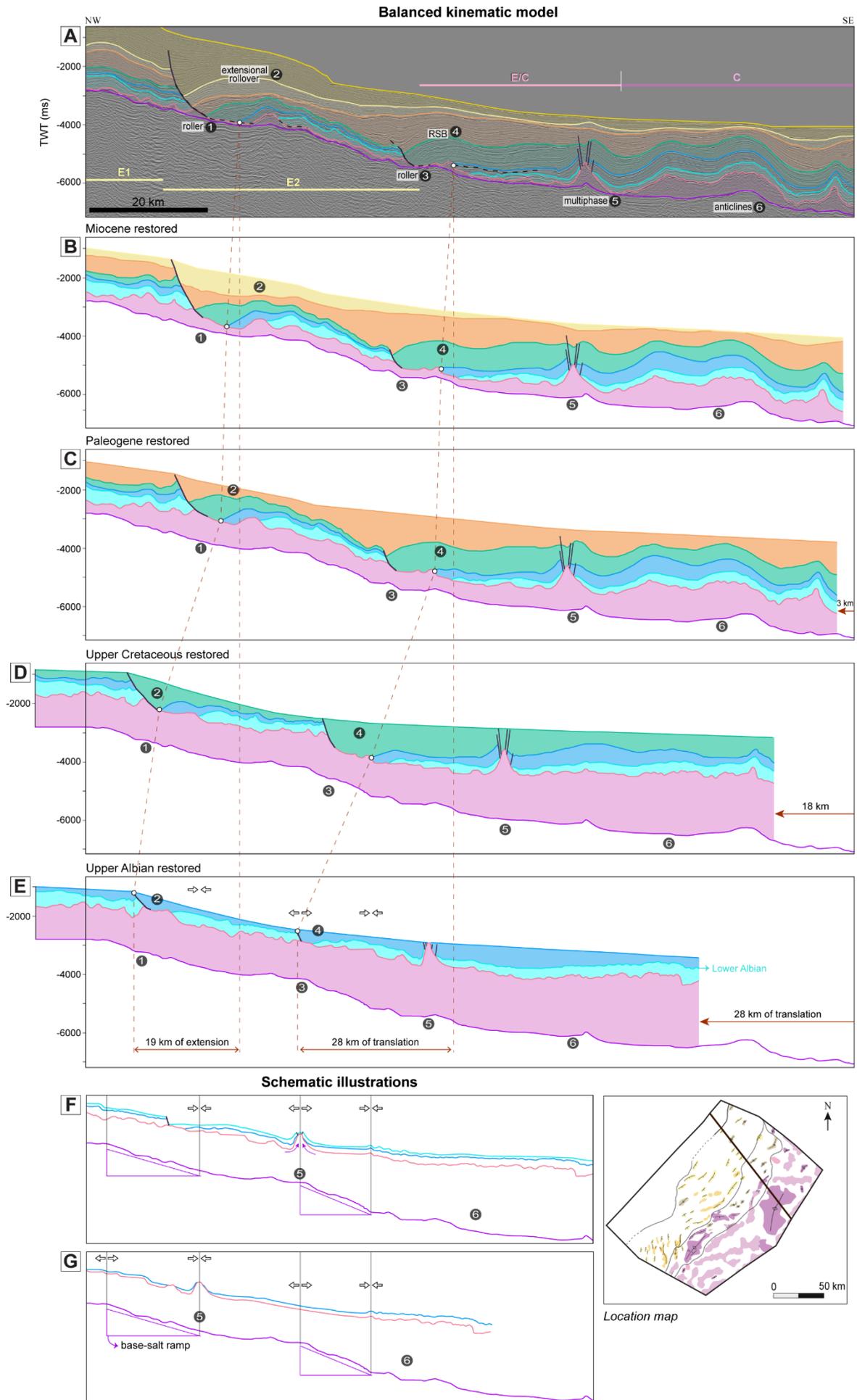
Location map — N; 0 50 km

Figure 10. (A) Interpreted seismic line 0239-0362 (see the map in the bottom right for location) used in the balanced kinematic model, shown in (B) to (E) – (B) is the restoration of the Miocene; (C) Paleogene; (D) Upper Cretaceous and (E) Upper Albian. See the methodology item for development details. (F) and (G) are schematic illustrations of salt deformation across base-salt ramps during the Albian. Salt and overburden structures are numbered to facilitate indications in the text. The dotted lines indicate the seaward salt movement (translation/extension). The colours of the horizons are indicated in Figures 2 and 7.

7 – Discussion

7.1. Base-salt relief as a control on salt tectonics

Even though the evaporites in the salt basins offshore SE Brazil were deposited during a period of relative tectonic quiescence, and the base-salt surface is overall quite smooth, there are a few large-displacement faults that offset this surface to form base-salt ramps with up to c. 2 km of relief. The major base-salt ramps in the study area are within the extensional domain, delineating the boundary between the External High and the External Low (Figures 2 and 4). The ramps are overall linear, but may be locally concave- or convex-seaward (Figure 4c), and are c. 20-180 km long, c. 3-20 km wide, have a maximum structural relief of c. 900 ms TWT (c. 2 km), and dip 3° to 9°. The more linear, elongate ramps trend NE, perpendicular to the regional salt translation direction. Most salt and overburden structures also trend NE, with exceptions to this observed to the southwest, downdip from the concave- or convex-seaward ramps, where extensional salt and overburden structures trend north (Figure 5c). This is likely related to: (a) local changes in base-salt structure further updip, outside of our dataset, which redirected the salt flow to be bi-directional or radial (Cobbold and Szatmari, 1991); and/or (b) the presence of numerous volcanic sills in this area (Figures 7e,f and 9), which caused local changes in overburden strength and thus deformation patterns (Magee et al., 2021).

In addition to influencing the *orientation* of salt and overburden structures, the geometry and scale of base-salt relief also affects the *types* of structures that form. For example, the extensional domain generally coincides with the area where the major base-salt ramps occur, near the boundary between the External High and the External Low (Figure 4d). More specifically, along-strike and down-dip zoning of the structures within the extensional domain

may reflect variations in the strain rate within the ductile salt layer, with locally steeper base-salt angles being associated with locally higher strain rates and the formation of salt rollers as opposed to extensional diapirs (Fort et al., 2004).

The multiphase (E/C) structures occur at the toe of the slope, on a relatively flat part of the base-salt surface adjacent to the External Low. Seaward translation of salt and its overburden across base-salt ramps from the high block (External High) to this low block (External Low), and the associated salt flux and volume variations, resulted in local belts of increased deformation (see Dooley et al., 2017). As the salt flows off a structural high onto a low, the salt flux decelerates as it encounters thick and slower-moving salt at the base of seaward-dipping ramps, ultimately generating local extensional hinges at the top of the ramps, and contractional hinges at the base (Dooley et al., 2017; 2018; Pichel et al., 2019a-b). This mechanism is responsible for triggering at least some of the contractional fold belts and anticlines in Campos Basin, and the subsequent extension of some of these structures. Dooley et al. (2017) interpreted a wide fold belt with polyharmonic folds in Campos Basin; these are is geometrically similar and, we infer, have a similar origin to the large antiform we identify in Figures 7b,c and 10 (see their figure 24 for comparison). It is important to stress that the multiphase evolution of the structures in the E/C domain are heterogeneous, and may go unnoticed in an isolated 2D analysis (e.g. Figure 9 - structure 1).

Through time, overburden structures on the high block of the External High become grounded due to salt welding, with extension migrating downdip, ultimately reaching the toe-of-slope. The migration of extension with time causes relatively late, relatively widespread (i.e. regional) extension of previously contractional structures and diapiric structures of the multiphase domain. This study shows that although classic models of gravity gliding and spreading on salt-influenced passive margins are broadly correct, they are rather oversimplified and fail to explain and adequately capture the diversity of salt and overburden structural styles

interpreted in the Campos Basin and elsewhere (cf., Evans and Jackson, 2019; Pichel et al., 2019a; Erdi and Jackson, 2021).

7.1.2. Estimating the magnitude and rate of salt-detached translation

Seaward gravity-driven translation of salt and its overburden in the Campos Basin started in the early Albian, lasting until at least the mid-Paleogene (Fig. 10). The distribution and evolution of key salt and overburden structures, and their relationship to base-salt relief, can constrain the magnitude of this translation.

RSBs have been used to determine the magnitude of salt-detached tectonic transport in passive margin basins, by measuring the distance between the top of the causal base-salt ramp and the (landward-directed) onlap point of the oldest intra-RSB strata (Jackson and Hudec, 2005; Pichel et al., 2018; Oppo et al., 2021). The RSBs in the Campos Basin are hybrid structures, evolving (in time) from and/or passing laterally (in space) into extensional rollovers due to ramp geometry, and temporal and spatial changes in salt thickness (see 5.1.2; Figure 10a-e). The hybrid extensional rollover-RSB in the NE (Figure 6c) started to form early in the Albian and was active until the mid-Neogene, recording post-Albian overburden extension of c. 19 km (Figure 10 – structure 2). The large, seaward RSB located further to the SW (Figure 6c) was active for a shorter period, containing Albian to mid-Paleogene growth strata, and recorded greater post-Albian translation (c. 28 km). Thus, the maximum seaward translation of the overburden recorded by the RSBs since the end of the Albian is c. 28 km, comparable to that calculated by Dooley et al. (2017) elsewhere in the Campos Basin (see their figure 24).

An alternative way to estimate the magnitude of horizontal translation in salt basins is by measuring the distance between the most seaward end of a train of high-frequency buckle folds and the base of a seaward-dipping, base-salt ramp inferred to have generated them (Dooley et al., 2017). Applying this methodology to our dataset, where such buckle folds may plausibly have developed during the Albian (i.e., the major seaward-dipping base-salt ramp in

the NW of the study area; see Figure 7b-d), we calculate translation magnitudes of c. 40 km (Figure 7b), c. 50 km (Figure 7c), and c. 60 km (Figure 7d) in the NE, centre, and SW of the study area, respectively. The horizontal translation magnitudes estimated from the stratigraphic analysis of the RSBs (c. 28 km) thus differs significantly to those based on the present position of overburden buckle folds with respect to their inferred causal ramps (c. 40-60 km). We argue that RSBs provide a more certain record of the magnitude of horizontal translation in salt basins for the following reasons: (i) the translation magnitude calculated from RSB analysis is more consistent with the magnitude of salt-detached extension measured in the updip domain (Figs. 8 and 10); (ii) the salt nappe emplaced on oceanic crust at the seaward end of the Campos Basin, and which is at least partly the expression of the amount of horizontal translation updip (see Jackson et al. 2015), is < 40 km wide (Figure 2b) (Davison et al. 2012), a value consistent with the magnitude of translation calculated from the RSBs; (iii) translation magnitudes calculated by RSB analysis in conjugate (i.e., Angolan; 13-23 km; Evans and Jackson, 2020; Erdi and Jackson, 2021) and neighbouring basins (i.e., Santos Basin; 28-32 km; Pichel et al., 2018) are more consistent with those defined here from comparable RSB analysis (c. 28 km); (iv) it is uncertain which ramp was responsible for the formation of the high-frequency buckle folds, i.e., was it the present toe-of-slope base-salt ramp or a more subtle ramp located further downdip?; (v) folding can occur due to regional overburden shortening and may not be diagnostic of translation. Based on this discussion, we infer that the Albian high-frequency folds in the multiphase domain (Figure 9 - structure 2) did not form at the same base of the base-salt ramp associated with the formation of the RSBs, but may have instead formed at one or more subtle ramps located further downdip (Figures 4c and 5).

Having argued that the *magnitude* of salt-detached translation in the Campos Basin is more likely c. 28 km than c. 40-60 km, we can now calculate the *duration* and *rate* of translation. Growth strata within the RSBs indicate translation started lasted until the middle Paleogene, defining post-Albian duration of c. 55 Ma and a translation rate of c. 0.5 mm/year.

Recent studies of RSBs in the conjugate Kwanza Basin, offshore Angola by Evans and Jackson (2019) and Erdi and Jackson (2021) demonstrate along-strike variability in both the magnitude and rate of Cenomanian-to-Recent salt-detached translation, i.e., from as little as 13 km at a rate of 0.13 mm/year in the NW of the study area, to 23.2 km at a rate of 0.23 mm/year in the SE. In the Santos Basin, offshore Brazil, Pichel et al. (2018) estimate a horizontal translation magnitude of 28-32 km lasting for c. 50 Myr (i.e., from the end-Albian until the middle Paleocene), thus defining a slightly faster translation rate than seen elsewhere (c. 0.7-0.8 mm/year). As argued by Pichel et al. (2018), Evans and Jackson (2019), and Erdi and Jackson (2021), this variability in the duration and rate of translation likely reflects changes in primary salt thickness and composition, the scale and distribution of base-salt relief, and local basement-involved tectonic processes driving salt-detached deformation (i.e., margin uplift) (see also Dooley et al., 2017). Some combination of these controls may explain along-strike variation in RSB development and evolution in the Campos Basin. For example, the base-salt surface is overall steeper in the SW compared to the NE (Figure 4d), and it is defined by wider and more numerous base-salt ramps (Figure 4c). Davison et al. (2012) also suggest the primary salt thickness increased south-westwards from c. 1.2 km to 2 km (see their figure 7), which is consistent with our observations that the magnitude of translation was greatest in the SW.

7.2. Implications for hydrocarbon exploration in the Campos Basin

The Campos Basin is the second most prolific hydrocarbon basin in Brazil, being responsible for c. 33% of the hydrocarbon production in Brazil (ANP real-time panel, accessed DATE 2021). The first oil discovery in the basin dates from 1970's, with the reservoir being Albian carbonates (Mohriak et al., 1990). Further exploration through the following decades led to the discovery of a further 41 oil and gas fields located 50-140 km off the Brazilian coast,

in water depths of 80-2400 m. The fields are associated with a range of plays and have reservoirs in a variety of stratigraphic units (Bruhn et al., 2003).

Known petroleum systems of the Campos Basin are composed of Barremian/Aptian (i.e. sub- to intrasalt) source rocks. Hydrocarbon migration from pre-rift source rocks to suprasalt reservoirs occurs through normal faults, or across areas of thin or welded salt (Guardado et al., 1989). The most important fields include reservoirs in post-salt turbidites located in various stratigraphic levels, for example the Albacora (Miocene), Marlim (Oligocene to Miocene), Barracuda (Oligocene to Eocene), and Roncador (Maastrichian) fields (Figure 1A for field locations) (Bruhn et al., 2003; ANP report, 2015). Salt-related faults form traps, controlling most of the oil and gas accumulations in these turbidite reservoirs (Bruhn et al., 2003; Mohriak et al., 2012). Subsalt reservoirs comprise rift (Barremian) and Aptian pre-salt carbonates ("coquinas") and clastics, and fractured syn-rift volcanics (Hauterivian) (Goldberg et al., 2017). The salt layer has a critical role for these deeper reservoirs, acting as an efficient seal rock.

The known post-salt reservoirs of the Campos Basin are mainly located within the thin-skinned extensional domain, which currently lies within relatively shallow water-depths (Figure 1a). This means significant unexplored areas may lie seaward of this location, in substantially deeper water. This study details the position and timing of salt-related deformation, key information required to push exploration further basinward into the multiphase and contractional domains. For example, we document multiwavelength salt anticlines in the multiphase domain (Albian – Top Cretaceous); these could represent structural traps, with later (end of the Cretaceous – Paleogene) extensional normal faults defining reservoir compartments (Figure 9 - structure 2). Hydrocarbon may have migrated from the pre-rift source rocks through welds adjacent to the large salt structures; given we infer these welds formed sometime during the end of the Cretaceous to the Paleogene, post-Paleogene migration is required to charge suprasalt traps, although the precise timing will vary based on the age of individual welds. High-frequency Albian buckle folds are common in the contractional domain (e.g. Figure 7b -

structure 4, 7c - structure 5) and can also create structural traps (Jackson and Hudec, 2017) for hydrocarbons sourced from suprasalt source rocks, if they are mature. Megaflaps flanking diapirs in the contractional domain (e.g. Figure 7a - structure 3, 7e - structure 8, 7f - structures 3 to SE), which began forming to the end of the Cretaceous, can compose three-way truncation traps against salt; megaflaps can also act as a lateral seal for stratigraphic traps and have implications for fluid pressures in minibasins (Rowan et al., 2016). Diapirs could also be flanked by Cretaceous to Paleogene deep-water clastic reservoirs in pinch-out traps at the margins of minibasins (e.g. Figure 7d - minibasin 6 and adjacent diapirs 5 and 7, 7e – minibasins 6 and flanking diapirs 5, 7 and 8), similar to discoveries in the Gulf of Mexico (Booth et al., 2003). Finally, turtle anticlines within salt-withdrawal basins (Cretaceous) (e.g. Figure 7c - structure 4) can cause structural inversion of stratigraphic units and can create stratigraphic/structural traps, similar to those documented in east Texas, US (Wescott and Hood, 1994).

7 - Conclusions

We use 2D and 3D seismic reflection and borehole data from the south-central Campos Basin to characterise salt-tectonic structural styles and related evolution of salt and overburden structures. The key conclusions of our study are:

- Variations in dip angle and direction in the base-salt surface define base-salt ramps, which define the boundary between the External High and the External Low, basement structures originated by rift tectonics. The dip angle of the base-salt ramps vary from 3° to 9°, and the dip direction trend broadly to NE, in overall linear geometries and locally concave-convex. The maximum structural relief of the ramps is c. 900 ms TWT (or c. 2 km).

- The distribution of the interpreted salt and overburden structures define three domains of thin-skinned, salt-detached deformation: extensional – subdivided into subdomains E1 and E2 –, contractional, and multiphase.

- We interpreted three multiphase structures: (i) contractional anticlines that were subjected to later extension and normal faulting; (ii) diapirs with passive and active growth later subjected to regional extension, developing landward-dipping normal faults on the landward flank; and, lastly, (iii) an extensional diapir that was subsequently squeezed. The structures in the multiphase domain formed in response to multiple, kinematically-variable (extensional and contractional) phases of deformation over time and space.

- Base-salt relief caused local variations in salt flux, affecting the regional domains of deformation, controlling or influencing the types of generated salt and overburden structures, and their evolution through time and space.

- Ramp syncline basins provide a record of c. 28 km horizontal translation of salt and its overburden in a rate of c. 0.5 mm/year from the end of the Albian to the middle Paleogene.

References

Amarante, F.B.d., Kuchle, J., Iacopini, D., Scherer, C.M.d.S., Alvarenga, R. dos S., Ene, P.L., Schilling, A.B., 2020. Seismic tectono-stratigraphic analysis of the Aptian pre-salt marginal system of Espírito Santo Basin, Brazil. Journal of South American Earth Sciences 98, 102474. https://doi.org/10.1016/j.jsames.2019.102474

ANP (Brazilian Agency for Petroleum, Natural Gas and Biofuels). 2015. Geological Summary and Sectors on Offer. Retrieved from http://rodadas.anp.gov.br/arquivos/Round_13/areas_oferecidas_r13/Sumarios_Geologicos/Sumario_Geologico_Bacia_Campos_R13.pdf

ANP Real-time Panel. 2021. Real-time web panel for production of oil and gas in Brazil. Retrieved from http://www.anp.gov.br/exploracao-e-producao-de-oleo-e-gas/paineis-dinamicos-de-producao-de-petroleo-e-gas-natural

ANP (Brazilian Agency for Petroleum, Natural Gas and Biofuels), Exploration and Production Database Web Maps – BDEP (Banco de Dados de Exploração e Produção). 2020. http://www.anp.gov.br/exploracao-e-producao-de-oleo-e-gas/dados-tecnicos

Baksi, A.K., 2018. Paraná flood basalt volcanism primarily limited to ~ 1 Myr beginning at 135 Ma: New 40 Ar/ 39 Ar ages for rocks from Rio Grande do Sul, and critical evaluation of published radiometric data. Journal of Volcanology and Geothermal Research 355, 66–77. https://doi.org/10.1016/j.jvolgeores.2017.02.016

Booth, J.R., Dean, M.C., DuVernay, A.E., III, Styzen, M.J., 2003. Paleo-bathymetric controls on the stratigraphic architecture and reservoir development of confined fans in the Auger Basin: central Gulf of Mexico slope. Marine and Petroleum Geology 20, 563–586. https://doi.org/10.1016/j.marpetgeo.2003.03.008

Bruhn, C.H.L., Gomes, J.A.T., Del Lucchese, C., Jr., Johann, P.R.S., 2003. Campos Basin: Reservoir Characterization and Management - Historical Overview and Future Challenges, in: Offshore Technology Conference. Presented at the Offshore Technology Conference, Offshore Technology Conference. https://doi.org/10.4043/15220-ms

Brun, J.-P., Fort, X., 2004. Compressional salt tectonics (Angolan margin). Tectonophysics 382, 129–150. https://doi.org/10.1016/j.tecto.2003.11.014

Brun, J.-P., Fort, X., 2011. Salt tectonics at passive margins: Geology versus models. Marine and Petroleum Geology 28, 1123–1145. https://doi.org/10.1016/j.marpetgeo.2011.03.004

Brun, J.-P., Mauduit, T.P.-O., 2009. Salt rollers: Structure and kinematics from analogue modelling. Marine and Petroleum Geology 26, 249–258. https://doi.org/10.1016/j.marpetgeo.2008.02.002

Chang, H.K., Kowsmann, R.O., Figueiredo, A.M.F., Bender, A., 1992. Tectonics and stratigraphy of the East Brazil rift system: an overview. Tectonophysics 213, 97–138.

Cobbold, P.R., Szatmari, P., 1991. Radial gravitational gliding on passive margins. Tectonophysics 188, 249–289. https://doi.org/10.1016/0040-1951(91)90459-6

Contreras, J., Zühlke, R., Bowman, S., Bechstädt, T., 2010. Seismic stratigraphy and subsidence analysis of the southern Brazilian margin (Campos, Santos and Pelotas basins). Mar. Petrol. Geol. 27 (9), 1952–1980.

Davison, I., 2007. Geology and tectonics of the South Atlantic Brazilian salt basins. Geological Society, London, Special Publications 272, 345–359. https://doi.org/10.1144/gsl.sp.2007.272.01.18

Davison, I., Alsop, I., Blundell, D., 1996. Salt tectonics: some aspects of deformation mechanics. Geological Society, London, Special Publications 100, 1–10. https://doi.org/10.1144/gsl.sp.1996.100.01.01

Davison, I., Anderson, L., Nuttall, P., 2012. Salt deposition, loading and gravity drainage in the Campos and Santos salt basins. Geological Society, London, Special Publications 363, 159–174. https://doi.org/10.1144/sp363.8

Demercian, S., Szatmari, P., Cobbold, P.R., 1993. Style and pattern of salt diapirs due to thin-skinned gravitational gliding, Campos and Santos basins, offshore Brazil. Tectonophysics 228 (3–4), 393–433.

Dooley, T.P., Hudec, M.R., Carruthers, D., Jackson, M.P.A., Luo, G., 2017. The effects of base-salt relief on salt flow and suprasalt deformation patterns — Part 1: Flow across simple steps in the base of salt. Interpretation 5, SD1–SD23. https://doi.org/10.1190/int-2016-0087.1

Erdi, A., Jackson, C.A.L., 2021. What Controls Contraction in the Translation Domain of the Outer Kwanza Basin, Offshore Angola? Basin Research. https://doi.org/10.1111/bre.12539

Evans, S.L., Jackson, C.A.L., 2019. Base-salt relief controls salt-related deformation in the Outer Kwanza Basin, offshore Angola. Basin Research 32, 668–687. https://doi.org/10.1111/bre.12390

Evans, S.L., Jackson, C.A.-L., 2021. Intra-salt structure and strain partitioning in layered evaporites: implications for drilling through Messinian salt in the eastern Mediterranean. Petroleum Geoscience petgeo2020-072. https://doi.org/10.1144/petgeo2020-072

Fetter, M., 2009. The role of basement tectonic reactivation on the structural evolution of Campos Basin, offshore Brazil: Evidence from 3D seismic analysis and section restoration. Marine and Petroleum Geology 26, 873–886. https://doi.org/10.1016/j.marpetgeo.2008.06.005

Fiduk, J.C., Rowan, M.G., 2012. Analysis of folding and deformation within layered evaporites in Blocks BM-S-8 & -9, Santos Basin, Brazil. Geological Society, London, Special Publications 363, 471–487. https://doi.org/10.1144/sp363.22

Fort, X., Brun, J.-P., Chauvel, F., 2004. Salt tectonics on the Angolan margin, synsedimentary deformation processes. Bulletin 88, 1523–1544. https://doi.org/10.1306/06010403012

Goldberg, K., Kuchle, J., Scherer, C.M.S., Alvarenga, R.S., Ene, P.L., Armelenti, G., De Ros, L.F., 2017. Re-Sedimented deposits in the rift section of the Campos Basin. Marine and Petroleum Geology 80, 412–431.

Guardado, L.R., Gamboa, L.A.P., Lucchesi, C.F., 1989. Petroleum geology of Campos Basin, Brazil: a model for producing Atlantic type basin. In: Edwards, J.D., Santagrossi, P.A. (Eds.), Divergent/Passive Margins Basins. AAPG Memoir 48, 3–36.

Guardado, L.R., Spadini, A.R., Brandão, J.S.L., Mello, M.R., 2000. Petroleum system of the Campos Basin, Brazil. In: Mello, M.R., Katz, B.J. (Eds.), Petroleum Systems of South Atlantic Margins. AAPG Memoir 73, 317–324.

Heilbron, M., Mohriak, W.U., Valeriano, C.M., Milani, E.J., Almeida, J., Tupinambá, M., 2000. From collision to extension: The roots of the southeastern continental margin of Brazil, in: Atlantic Rifts and Continental Margins. American Geophysical Union, pp. 1–32. https://doi.org/10.1029/gm115p0001

Hudec, M.R., Jackson, M.P.A., Schultz-Ela, D.D., 2009. The paradox of minibasin subsidence into salt: Clues to the evolution of crustal basins. Geological Society of America Bulletin 121, 201–221. https://doi.org/10.1130/B26275.1

Jackson, C.A. -L., Duffy, O.B., Fernandez, N., Dooley, T.P., Hudec, M.R., Jackson, M.P.A., Burg, G., 2019. The stratigraphic record of minibasin subsidence, Precaspian Basin, Kazakhstan. Basin Research 32, 739–763. https://doi.org/10.1111/bre.12393

Jackson, C.A.-L., Jackson, M.P.A., Hudec, M.R., 2015. Understanding the kinematics of salt-bearing passive margins: A critical test of competing hypotheses for the origin of the Albian Gap, Santos Basin, offshore Brazil. Geological Society of America Bulletin 127, 1730–1751. https://doi.org/10.1130/b31290.1

Jackson, M.P.A., Hudec, M.R., 2005. Stratigraphic record of translation down ramps in a passive-margin salt detachment. Journal of Structural Geology 27, 889–911. https://doi.org/10.1016/j.jsg.2005.01.010

Jackson, M. P. A., Hudec, M. R., 2017. Salt Tectonics: Principles and Practice. Cambridge: Cambridge University Press. https://doi.org/10.1017/9781139003988

Hudec, M.R., Norton, I.O., Jackson, M.P.A., Peel, F.J., 2013. Jurassic evolution of the Gulf of Mexico salt basin. AAPG Bulletin 97, 1683–1710. https://doi.org/10.1306/04011312073

Kukla, P.A., Strozyk, F., Mohriak, W.U., 2018. South Atlantic salt basins – Witnesses of complex passive margin evolution. Gondwana Research 53, 41–57. https://doi.org/10.1016/j.gr.2017.03.012

Lundin, E.R., 1992. Thin-skinned extensional tectonics on a salt detachment, northern Kwanza Basin, Angola. Marine and Petroleum Geology 9, 405–411. https://doi.org/10.1016/0264-8172(92)90051-f

Magee, C., Pichel, L.M., Madden-Nadeau, A.L., Jackson, C.A. -L., Mohriak, W., 2021. Salt–magma interactions influence intrusion distribution and salt tectonics in the Santos Basin, offshore Brazil. Basin Research. https://doi.org/10.1111/bre.12537

Marfurt, K.J., Alves, T.M., 2015. Pitfalls and limitations in seismic attribute interpretation of tectonic features. Interpretation 3, SB5–SB15. https://doi.org/10.1190/int-2014-0122.1

Meisling, K.E., Cobbold, P.R., Mount, V.S., 2001. Segmentation of an obliquely rifted margin, Campos and Santos basins, southeastern Brazil. AAPG Bulletin 85 (11), 1903–1924.

Mohriak, W.U., Mello, M.R., Karner, G.D., Dewey, J.F., Maxwell, J.R., 1989. Structural and stratigraphic evolution of the Campos Basin, offshore Brazil. In: Tankard, A.J., Balkwill, H.R. (Eds.), Extensional Tectonics and Stratigraphy of the North Atlantic Margins. AAPG Memoir 46, 577–598.

Mohriak, W.U., Mello, M.R., Dewey, J.F., Maxwell, J.R., 1990. Petroleum geology of the Campos Basin, offshore Brazil. Geological Society, London, Special Publications 50, 119–141. https://doi.org/10.1144/gsl.sp.1990.050.01.07

Mohriak, W., Nemčok, M., Enciso, G., 2008. South Atlantic divergent margin evolution: rift-border uplift and salt tectonics in the basins of SE Brazil. Geological Society, London, Special Publications 294, 365–398. https://doi.org/10.1144/sp294.19

Mohriak, W.U., Szatmari, P., Anjos, S., 2012. Salt: geology and tectonics of selected Brazilian basins in their global context. Geological Society, London, Special Publications 363, 131–158. https://doi.org/10.1144/sp363.7

Oppo, D., Evans, S., Iacopini, D., Kabir, S.M.M., Maselli, V., Jackson, C.A. -L., 2021. Leaky salt: Pipe trails record the history of cross-evaporite fluid escape in the northern Levant Basin, Eastern Mediterranean. Basin Research. https://doi.org/10.1111/bre.12536

Peel, F.J., 2014. How do salt withdrawal minibasins form? Insights from forward modelling, and implications for hydrocarbon migration. Tectonophysics 630, 222–235. https://doi.org/10.1016/j.tecto.2014.05.027

Pichel, L.M., Peel, F., Jackson, C.A.-L., Huuse, M., 2018. Geometry and kinematics of salt-detached ramp syncline basins. Journal of Structural Geology 115, 208–230. https://doi.org/10.1016/j.jsg.2018.07.016

Pichel, L.M., Jackson, C.A.L., Peel, F., Dooley, T.P., 2019a. Base-salt relief controls salt-tectonic structural style, São Paulo Plateau, Santos Basin, Brazil. Basin Research 32, 453–484. https://doi.org/10.1111/bre.12375

Pichel, L.M., Finch, E., Gawthorpe, R.L., 2019b. The Impact of Pre-Salt Rift Topography on Salt Tectonics: A Discrete-Element Modeling Approach. Tectonics 38, 1466–1488. https://doi.org/10.1029/2018tc005174

Pichel, L.M., Jackson, C.A.-L., 2020. The enigma of the Albian Gap: spatial variability and the competition between salt expulsion and extension. Journal of the Geological Society 177, 1129–1148. https://doi.org/10.1144/jgs2020-055

Quirk, D.G., Hertle, M., Jeppesen, J.W., Raven, M., Mohriak, W.U., Kann, D.J., Nørgaard, M., Howe, M.J., Hsu, D., Coffey, B., Mendes, M.P., 2013. Rifting, subsidence and continental break-up above a mantle plume in the central South Atlantic. Geological Society, London, Special Publications 369, 185–214. https://doi.org/10.1144/sp369.20

Quirk, D.G., Schødt, N., Lassen, B., Ings, S.J., Hsu, D., Hirsch, K.K., Von Nicolai, C., 2012. Salt tectonics on passive margins: examples from Santos, Campos and Kwanza basins. Geological Society, London, Special Publications 363, 207–244. https://doi.org/10.1144/sp363.10

Rangel, H.D., Martins, F.A.L., Esteves, F.R., Feijó, F.J., 1994. Bacia de Campos. Boletim de Geociências da Petrobras 8 (1), 203–218.

Rowan, M.G., Peel, F.J., Vendeville B.C., 2004, Gravity-driven fold belts on passive margins. In McClay, K.K. (Eds.), Thrust tectonics and hydrocarbon systems: AAPG Memoir 82, 157–182.

Rowan, M.G., Ratliff, R.A., 2012. Cross-section restoration of salt-related deformation: Best practices and potential pitfalls. Journal of Structural Geology 41, 24–37. https://doi.org/10.1016/j.jsg.2011.12.012

Rowan, M.G., 2014. Passive-margin salt basins: hyperextension, evaporite deposition, and salt tectonics. Basin Research 26, 154–182. https://doi.org/10.1111/bre.12043

Rowan, M.G., Giles, K.A., Hearon IV, T.E., Fiduk, J.C., 2016. Megaflaps adjacent to salt diapirs. Bulletin 100, 1723–1747. https://doi.org/10.1306/05241616009

Sclater, J.G., Christie, P.A.F., 1980. Continental stretching: An explanation of the Post-Mid-Cretaceous subsidence of the central North Sea Basin. J. Geophys. Res. 85, 3711–3739. https://doi.org/10.1029/jb085ib07p03711

Szatmari, P., 2000. Habitat of petroleum along the South Atlantic margins. In: Mello, M.R., Katz, B.J. (Eds.), Petroleum Systems of South Atlantic Margins: AAPG Memoir 73, 69–75.

Trusheim, F., 1960. Mechanism of salt migration in northern Germany. AAPG Bulletin 44, 1519–1540.

Vendeville, B.C., Jackson, M.P.A., 1992 a. The rise of diapirs during thin-skinned extension. Marine and Petroleum Geology 9, 331–354. https://doi.org/10.1016/0264-8172(92)90047-i

Vendeville, B.C., Jackson, M.P.A., 1992 b. The fall of diapirs during thin-skinned extension. Marine and Petroleum Geology 9, 354–371. https://doi.org/10.1016/0264-8172(92)90048-j

Wescott, W.A., Hood, W.C., 1994. Hydrocarbon Generation and Migration Routes in the East Texas Basin. Bulletin 78. https://doi.org/10.1306/bdff908c-1718-11d7-8645000102c1865d

Winter, W.R., Jahnert, R.J., França, A.B., 2007. Bacia de Campos. Boletim de Geociências da Petrobras 15(2), 511–529.